VIROLOGY

Hepatovirus translation requires PDGFA-associated protein 1, an eIF4E-binding protein regulating endoplasmic reticulum stress responses

Takayoshi Shirasaki[1], Erik Lenarcic[2], Ichiro Misumi[3], Ling Xie[4], William G. Fusco[5], Bryan Yonish[1], Anshuman Das[1]†, Hyejeong Kim[2]‡, Craig E. Cameron[2], Mélissa Léger-Abraham[6,7], Xian Chen[1,4], John M. Cullen[8], Jason K. Whitmire[1,3], You Li[1,5], Joseph A. Duncan[1,5], Nathaniel J. Moorman[1,2], Stanley M. Lemon[1,2,5]*

The overexpression and misfolding of viral proteins in the endoplasmic reticulum (ER) may cause cellular stress, thereby inducing a cytoprotective, proteostatic host response involving phosphorylation of eukaryotic translation initiation factor 2 subunit alpha (eIF2α). Here, we show that hepatitis A virus, a positive-strand RNA virus responsible for infectious hepatitis, adopts a stress-resistant, eIF2α-independent mechanism of translation to ensure the synthesis of viral proteins within the infected liver. Cap-independent translation directed by the hepatovirus internal ribosome entry site and productive hepatovirus infection of mice both require platelet-derived growth factor subunit A (PDGFA)–associated protein 1 (PDAP1), a small phosphoprotein of unknown function with eIF4E-binding activity. PDAP1 also interacts with eIF1A and is essential for translating stress-resistant host messenger RNAs that evade the proteostatic response to ER stress and that encode proteins promoting the survival of stressed cells.

INTRODUCTION

Hepatitis A virus (HAV) is an atypical picornavirus associated with both epidemic and sporadic enterically transmitted hepatitis in humans (*1*). Like all picornaviruses, its single-stranded positive-sense 7.5-kb RNA genome lacks a eukaryotic 5′ 7-methylguanosine (m^7G) cap. Translation of a single large open reading frame initiates internally, 740 nucleotides from the 5′ end of the RNA, under the control of an upstream internal ribosome entry site (IRES) that is structurally distinct and functionally less efficient than the poliovirus (PV) and other well-studied picornaviral IRES elements (*2*–*4*). Although translation is cap-independent, previous biochemical studies have revealed an unexpected and poorly understood requirement for the cap-binding protein, eukaryotic translation initiation factor 4E (eIF4E), and its binding site within the scaffold protein, eIF4G (*4*–*6*). HAV IRES-directed translation is also abolished in vitro in the presence of m^7GpppG cap analog, suggesting that the cap-binding pocket of eIF4E may need to be empty for HAV translation to proceed (*5*, *6*). This unusual eIF4E-dependent IRES-initiated translation is rate limiting for replication of the virus (*7*). Genome-wide CRISPR screens suggest that numerous translation-related proteins are essential for HAV replication (*8*, *9*), including eIF4B, components of the multi-subunit eIF3 complex (eIF3A, 3C, 3CL, 3F, 3G, and 3 M), and polypyrimidine tract binding protein 1 (PTBP1), which is known to transactivate the HAV IRES (*10*). Such a preponderance of translation factors has not been identified in similar screens for host factors of other picornaviruses (*11*, *12*).

CRISPR screens also point to an essential yet unexplained role for platelet-derived growth factor subunit A (PDGFA)–associated protein 1 (PDAP1, also known as 28-kDa heat- and acid-stable phosphoprotein) in HAV infection (fig. S1, A and B) (*8*, *9*). This protein is evolutionarily conserved and expressed in all tissues but has no defined function. Previous studies suggest that PDAP1 is a casein kinase II (CK2) substrate (*13*) and may interact with PDGF (*14*). Recent reports link increased PDAP1 expression to gastric and rectal carcinomas (*15*, *16*) and malignant glioma progression (*17*) and show that it is regulated transcriptionally by the proto-oncogene protein c-Myc (*18*). Murine and human PDAP1 proteins share 97% amino acid identity (175/181 residues), and targeted depletion of PDAP1 in murine mucosal epithelial cells exacerbates dextran sulfate sodium–induced colitis, promoting development of colon cancer (*18*). PDAP1 depletion also promotes stress-induced death of murine B cells ex vivo (*19*). Both phenotypes suggest an association with cellular stress responses, but neither phenotype is well explained.

Here, we report that PDAP1 is an indispensable HAV host factor required for replication in cell culture and productive infection in a murine model of hepatitis A. We show that PDAP1 is required for translation of HAV RNA, interacts with human eIF4E as well as the translation initiation factor eIF1AX, and is required in mice for the expression of proteins that promote cell survival in the face of endoplasmic reticulum (ER) stress.

RESULTS

HAV infection of PDAP1-deficient cells

To confirm HAV requires PDAP1 for its replication, we used CRISPR-Cas9 to establish Huh-7.5 hepatoma cell lines deficient in PDAP1

[1]Lineberger Comprehensive Cancer Center, The University of North Carolina at Chapel Hill, Chapel Hill, NC, USA. [2]Department of Microbiology and Immunology, The University of North Carolina at Chapel Hill, Chapel Hill, NC, USA. [3]Department of Genetics, The University of North Carolina at Chapel Hill, Chapel Hill, NC, USA. [4]Department of Biochemistry and Biophysics, The University of North Carolina at Chapel Hill, Chapel Hill, NC, USA. [5]Department of Medicine, The University of North Carolina at Chapel Hill, Chapel Hill, NC, USA. [6]Division of Molecular Medicine, Harvard Medical School, Boston, MA, USA. [7]Department of Microbiology, Blavatnik Institute, Harvard Medical School, Boston, MA, USA. [8]College of Veterinary Medicine, North Carolina State University, Raleigh, NC, USA.
*Corresponding author. Email: smlemon@med.unc.edu
†Present address: Lentigen Technology Inc., Gaithersburg, MD 20878, USA.
‡Present address: CBRN Defense Research Institute, Seoul, Republic of Korea.

expression: PDAP1-KO1.04 and PDAP1-KO2 (Fig. 1A). These cell lines, produced with guide sgRNAs targeting *PDAP1* exons 4 and 2, respectively, proliferated well without growth defect. When infected with either naked or quasi-enveloped HAV (*20*), PDAP1-KO1.4 cells produced 50- to 75-fold less viral RNA than control cells (sgCtrl) transduced with nontargeting sgRNA (Fig. 1B and fig. S1C). Similarly, replication of a nanoluciferase (NLuc)–expressing reporter virus (18f-NLuc) (*21*) was ablated in both PDAP1-KO1.4 and PDAP1-KO2 cells, with infectious virus yields reduced over 100-fold by 24 hours after infection (Fig. 1, C and D, and fig. S1D). Transient lentivirus expression of PDAP1 significantly rescued replication in the knockout (KO) cells and also caused increases in viral RNA in sgCtrl control cells (Fig. 1, B to D, and fig. S1C). Collectively, these data show that HAV replication is dependent on PDAP1 in hepatoma

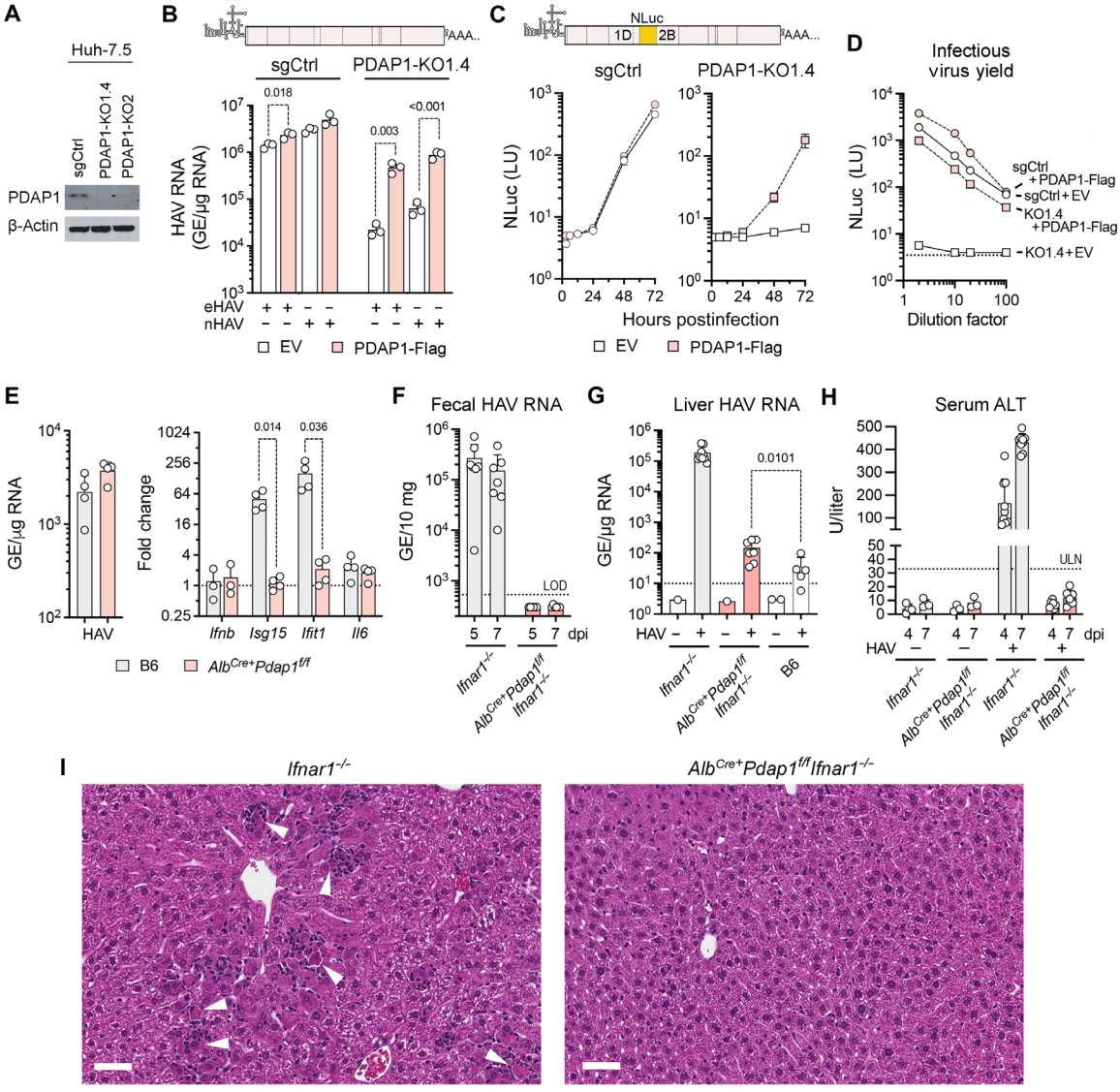

Fig. 1. PDAP1 is an essential hepatovirus host factor. (**A**) Immunoblots showing PDAP1 expressed in PDAP1-deficient (PDAP1-KO1.4 and PDAP1-KO-2) versus control (sgCtrl) cells transduced with nontargeting sgRNA. (**B**) HAV RNA quantified by RT-PCR in PDAP1-KO1.4 and control sgCtrl cells 72 hours after inoculation of gradient-purified quasi-enveloped (eHAV) or naked (nHAV) 18f virus. Cells were transduced with PDAP1-Flag–expressing lentivirus or empty vector (EV) prior to HAV challenge. (**C**) NLuc expressed by the 18f-NLuc reporter virus in PDAP1-KO1.4 versus sgCtrl cells, with or without PDAP1 reconstituted as in (B). LU, light units. (**D**) Infectious virus released from PDAP1-KO1.4 and sgCtrl cells 24 hours after infection [with and without PDAP1 reconstitution as in (C)] was quantified by inoculating dilutions of cell culture supernatant fluids onto naïve Huh-7.5 cells, with NLuc activity measured 72 hours later. Data shown in (B) to (D) are means ± SD of $N = 3$ technical replicates from representative experiments. (**E**) (Left) HAV RNA abundance and (right) fold change in innate immune response gene transcript abundance 15 hours after intravenous virus challenge of male *Alb*$^{Cre+}$*Pdap1*$^{f/f}$ or B6 mice. $N = 4$, *P* values by two-sided *t* test. GE, genome equivalents. (**F**) HAV RNA abundance in feces of male *Ifnar1*$^{-/-}$ versus *Alb*$^{Cre+}$*Pdap1*$^{f/f}$*Ifnar1*$^{-/-}$ mice ($N = 5$ to 6) determined by RT-qPCR 5 and 7 days after virus inoculation (dpi). LOD, limit of detection. (**G**) Viral RNA abundance in livers of male *Ifnar1*$^{-/-}$, *Alb*$^{Cre+}$*Pdap1*$^{f/f}$*Ifnar1*$^{-/-}$, or B6 mice ($N = 5$ to 8) inoculated with 2×10^6 GE virus 7 dpi. *P* value by two-sided Mann-Whitney test. (**H**) Serum ALT activities in *Ifnar1*$^{-/-}$ or *Alb*$^{Cre+}$*Pdap1*$^{f/f}$*Ifnar1*$^{-/-}$ mice 4 and 7 dpi. ULN, upper limit of normal. Each symbol in (E) and (F) represents an individual animal; columns represent means ± SD. (**I**) Representative H&E-stained sections of livers from *Ifnar1*$^{-/-}$ or *Alb*$^{Cre+}$*Pdap1*$^{f/f}$*Ifnar1*$^{-/-}$ mice 7 days after intravenous virus challenge. Arrows denote apoptotic hepatocytes with surrounding inflammatory cells. Scale bars, 50 μm.

cells. By contrast, a PV reporter virus, PV1-NLuc, replicated well in the absence of PDAP1 (fig. S1E), indicating that PDAP1 is not universally required by picornaviruses.

To assess the requirement for PDAP1 in replication of HAV in vivo, we bred C57BL/6 (B6) mice with a conditional floxed *Pdap1*^{f} allele (*19*) to *Alb*$^{Cre+}$ mice expressing Cre recombinase under the control of the mouse albumin promoter to produce *Alb*$^{Cre+}$*Pdap1*$^{f/f}$ mice with hepatocyte-specific *Pdap1* deletion. These mice had normal liver histology but were smaller than B6 mice and had low serum protein concentrations and elevated serum alkaline phosphatase activity (fig. S2, A to D). Although wild-type B6 mice are generally nonpermissive for HAV infection, intravenous virus challenge generates a brisk intrahepatic innate immune response marked by induction of multiple interferon-stimulated genes in response to transient virus replication (*22*). This innate immune response to HAV challenge was miniscule in *Alb*$^{Cre+}$*Pdap1*$^{f/f}$ mice compared with B6 mice, consistent with the absence of any virus replication (Fig. 1E and fig. S2E). By contrast, there was no deficit in the innate immune response to lymphocytic choriomeningitis virus (LCMV), which is unrelated to HAV, in *Alb*$^{Cre+}$*Pdap1*$^{f/f}$ mice (fig. S2, F and G).

To directly demonstrate a defect in viral replication, we crossed *Alb*$^{Cre+}$*Pdap1*$^{f/f}$ mice with *Ifnar1*$^{-/-}$ mice that lack the type I interferon receptor and are highly permissive for HAV infection (*23*, *24*). The *Alb*$^{Cre+}$*Pdap1*$^{f/f}$*Ifnar1*$^{-/-}$ mice produced by the cross were similar in size to *Alb*$^{Cre+}$*Pdap1*$^{f/f}$ mice and showed similar abnormalities in serum chemistries (fig. S2D). Unlike *Ifnar1*$^{-/-}$ mice, they were completely refractory to infectious challenge with HAV (Fig. 1, F to H). Whereas *Ifnar1*$^{-/-}$ mice demonstrated robust fecal shedding of virus produced in the liver following intravenous virus challenge (*23*), there was no detectable virus shedding from *Alb*$^{Cre+}$*Pdap1*$^{f/f}$*Ifnar1*$^{-/-}$ mice (Fig. 1F). Moreover, the amount of viral RNA present in livers of *Alb*$^{Cre+}$*Pdap1*$^{f/f}$*Ifnar1*$^{-/-}$ mice 7 days after inoculation was minimally increased over wild-type B6 mice and 1000-fold less than that present in sex-matched *Ifnar1*$^{-/-}$ controls (Fig. 1G). Serum alanine aminotransferase (ALT) activity and liver histology remained normal in *Alb*$^{Cre+}$*Pdap1*$^{f/f}$*Ifnar1*$^{-/-}$ mice, whereas ALT rose >50-fold in association with widespread inflammation and hepatocellular apoptosis in livers of similarly inoculated *Ifnar1*$^{-/-}$ mice (Fig. 1, H and I). Collectively, these data reveal a remarkable, near-absolute requirement for PDAP1 in HAV infection and pathogenesis.

PDAP1 and cap-independent translation of HAV RNA

Despite the inability of HAV to infect PDAP1-deficient cells (Fig. 1, A and B), there was no deficit in attachment or entry of either quasi-enveloped or naked virus (Fig. 2A). By contrast, a subgenomic HAV replicon RNA (HAV-FLuc) lacking capsid protein-coding sequence generated low initial luciferase reporter levels following transfection into PDAP1-KO1.4 cells and subsequently failed to replicate (Fig. 2B). Because there was no reduction in the stability of electroporated HAV RNA in these cells (Fig. 2C), the low initial expression of luciferase by the replicon suggests a primary defect in translation of the RNA. To directly assess the activity of the IRES, we transfected cells with a reporter plasmid containing a split green fluorescent protein (GFP) sequence and intronic sequences that drive the production of backspliced circular RNA (circRNA) transcripts containing the HAV IRES (Fig. 2D) (*25*–*27*). GFP can be synthesized from these transcripts only by IRES-mediated translation of the backspliced circRNA in which the continuity of the GFP sequence is restored. The efficiency of translation in PDAP1-replete or PDAP1-deficient cells was calculated by normalizing the quantity of GFP detected in immunoblots to RNA abundance determined by a reverse transcription polymerase chain reaction (RT-PCR) assay specific for circular transcripts (*27*). Notably, the HAV circRNA IRES reporter was inactive in PDAP1-KO1.4 cells, with only 6.4 ± 3% SEM of its activity in control sgCtrl cells (Fig. 2, E and F). Similar circRNA IRES reporters revealed a severe defect in translation initiated by the Kaposi's sarcoma-associated herpesvirus (KSHV) IRES (23 ± 9% SEM; Fig. 2, E and F), which, like the HAV IRES, has been suggested to require eIF4E (*28*). The PV IRES (34 ± 10% SEM) and encephalomyocarditis virus (EMCV) IRES (37 ± 10% SEM) were less severely impaired. In contrast, the hepatitis C virus (HCV) IRES, which, unlike these other IRES elements, binds 40*S* ribosomes directly and does not require eIF4A or eIF4G (*29*, *30*), showed no impairment in the absence of PDAP1.

Polysome profiling on 10 to 50% sucrose gradients confirmed the circRNA reporter results, revealing a failure of HAV translation initiation in PDAP1-deficient cells, with no loading of HAV RNA onto 80*S* ribosomes and polysomes and the highest HAV RNA abundance in fractions sedimenting <40*S* (Fig. 2G, top panel). Translational efficiency, defined as the percentage of HAV RNA associated with polysomes, was reduced from 74 to 79% to 10 to 26% in two independent experiments (Fig. 2H). By contrast, the translational efficiency of β-actin mRNA was unchanged in PDAP1-deficient cells (Fig. 2H). The defect in HAV translation was corrected by transient expression of PDAP1-Flag (translation efficiency increasing to 75%) (Fig. 2G, top panel). The Flag-tagged PDAP1 migrated with the polysome fraction in PDAP1-replete cells, indicating an association with translating ribosomes from which it could be released by EDTA (Fig. 2G, bottom panel). Despite the defect in HAV translation, global protein synthesis, measured by [^{35}S]-Met/Cys incorporation, was not measurably diminished in uninfected PDAP1-deficient cells (Fig. 2I). [^{35}S]-Met/Cys incorporation was reduced by ~50% in HAV-infected sgCtrl cells, consistent with a cytopathic viral effect (*31*). However, there was no reduction in PDAP1-deficient cells inoculated with HAV (Fig. 2I), in line with the lack of viral replication in these cells.

eIF4E-binding activity of PDAP1

AlphaFold2 structural modeling (*32*) predicts that much of PDAP1 is intrinsically disordered, with an extended C-terminal coil broken by a glycine at residue 131 (Fig. 3A). Residues 124 to 130 comprise a canonical tyrosine eIF4E-binding motif (YXXXXLΦ, where Φ is hydrophobic) found in eIF4E-binding proteins such as 4E-BP1 and eIF4G (Fig. 3B) (*33*). The PDAP1 motif has Ala as the hydrophobic residue instead of Leu or Met present in other eIF4E-binding proteins and shares conserved basic residues at −3 and +2 positions relative to Tyr. Consistent with this motif in PDAP1, eIF4E efficiently coimmunoprecipitated with PDAP1-Flag expressed in either infected or uninfected cells (Fig. 3C). Moreover, purified recombinant His-tagged PDAP1 expressed in bacteria was pulled down by affinity purification using a glutathione *S*-transferase (GST)–tagged eIF4E, whereas in a reciprocal experiment, GST-eIF4E coimmunoprecipitated with recombinant His-PDAP1 (Fig. 3D). The ability of GST-eIF4E to pull down ectopically expressed PDAP1-Flag was eliminated by a Tyr^{124} to Ala substitution (Y124A) that ablates the eIF4E-binding motif (Fig. 3E). This result suggests a direct interaction between PDAP1 and eIF4E through the motif. Confirming the importance of this interaction to HAV translation, ectopically

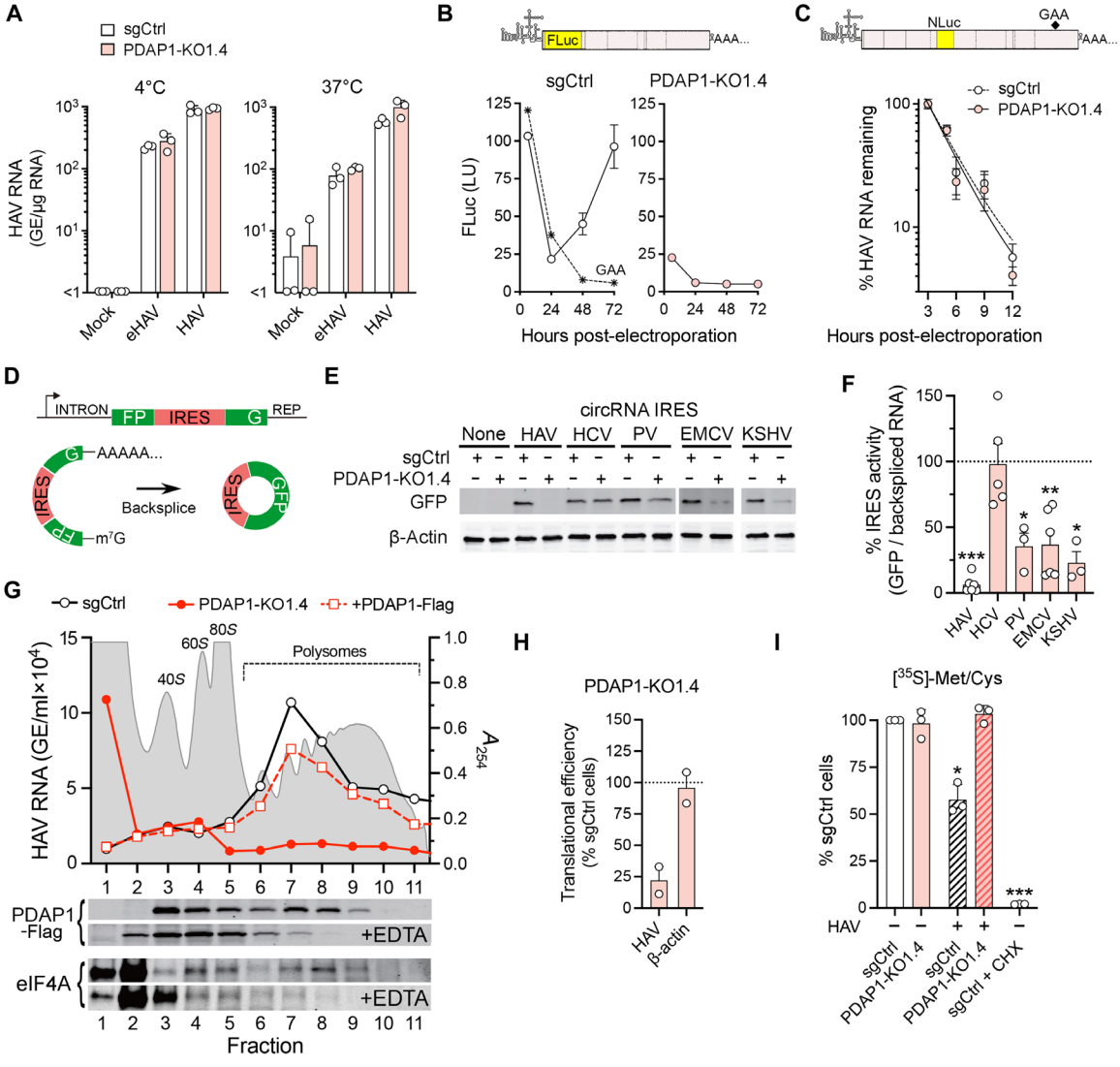

Fig. 2. PDAP1 is required for HAV IRES-mediated translation. (**A**) (Left) Quasi-enveloped (eHAV) and naked virus (nHAV) attached to control sgCtrl and PDAP1-KO1.4 cells at 4°C, measured by RT-PCR. (Right) Cell uptake of HAV at 37°C. GE, genome equivalent. (**B**) FLuc expressed by sub-genomic HAV replicon RNA. GAA, lethal 3D^{pol} mutation. (**C**) HAV RNA decay in sgCtrl and PDAP1-KO1.4 cells electroporated with 18f viral RNA containing a lethal 3D^{pol} mutation. RNA abundance measured by RT-qPCR. Data are means ± SD of $N = 3$ technical replicates. (**D**) circRNA IRES reporter transcript with split G/FP sequence flanking the IRES and upstream intron and downstream inverse repeat sequences (REP) driving backsplicing. (**E**) Immunoblots of GFP expressed by HAV, HCV, PV, EMCV, and KSHV circRNA IRES reporter plasmids transfected into sgCtrl or PDAP1-KO1.4 cells. (**F**) IRES-mediated translation efficiency in PDAP1-KO1.4 versus sgCtrl cells (100%), calculated as GFP/GAPDH abundance normalized to circRNA transcripts quantified by specific RT-qPCR. Data are means ± SEM from $N = 3$ to 6 independent transfections. *$P < 0.05$; **$P < 0.01$; ***$P < 0.001$, by one-sample *t* test and Wilcoxon test. (**G**) HAV RNA associated with polysomes in sgCtrl cells, PDAP1-KO1.4 cells, or PDAP1-KO1.4 cells transduced with lentivirus expressing PDAP1-Flag. Cells were harvested 5 hours after infection, and ribosomes were separated on a 10 to 50% sucrose gradient. Below are immunoblots of PDAP1-Flag and eIF4E in fractions from HAV-infected PDAP1-KO1.4 cells expressing PDAP1-Flag, with and without 50 mM EDTA. (**H**) Translation efficiency (percent RNA associated with polysomes) of HAV and β-actin mRNA in PDAP1-KO1.4 cells, relative to sgCtrl cells (100%) in two independent experiments. (**I**) [^{35}S]-Met/Cys incorporated into trichloroacetic acid–precipitable material over 30-min incubation in PDAP1-KO1.4 cells normalized to sgCtrl cells (100%), with or without HAV infection. CHX, 100 µg/ml cycloheximide (CHX). Data are means ± SD of $N = 3$ technical replicates. *$P < 0.05$; **$P < 0.01$; ***$P < 0.001$, by *t* test.

expressing Flag-tagged PDAP1-Y124A failed to rescue circRNA HAV IRES reporter activity (Fig. 3F) or HAV replication (Fig. 3G) in PDAP1-KO1.4 cells. Collectively, these data suggest that PDAP1 is a previously unrecognized eIF4E-binding protein and that the PDAP1/eIF4E interaction is crucial for hepatovirus translation and replication. The interaction of PDAP1 with eIF4E was not affected by the addition of a cap analog (m^7GTP) (fig. S3A), consistent with a previous structural study showing that peptides representing the tyrosine eIF4E-binding motif interact with a pair of helices on the dorsal convex surface of eIF4E, 35 Å distant from the cap-binding pocket (*33*).

Phospho-regulation of PDAP1

Because the structure and affinity of eIF4E-binding protein for eIF4E is tightly regulated by phosphorylation (*34*, *35*), the affinity of PDAP1 for eIF4E, and by extension its capacity to support HAV

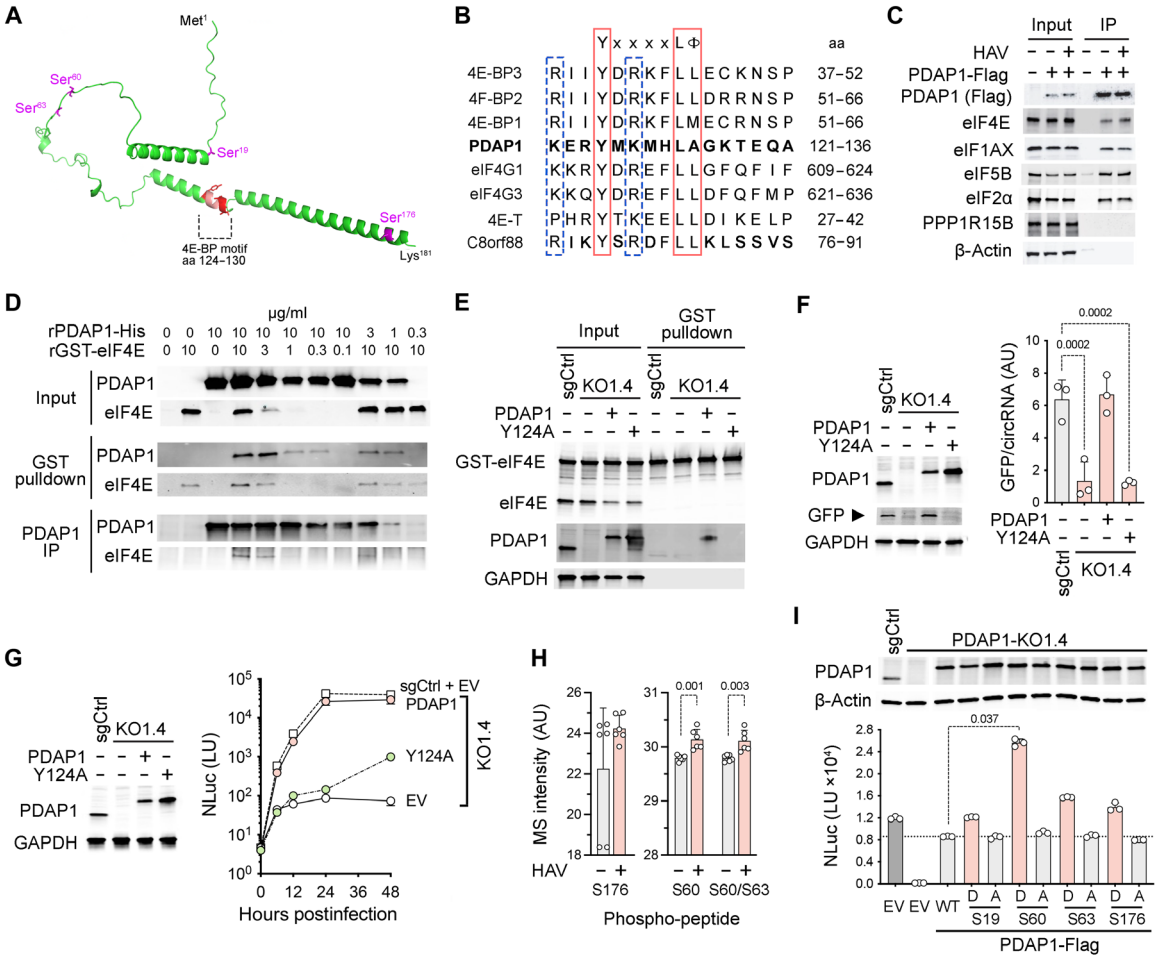

Fig. 3. PDAP1 is an eIF4E-binding protein. (**A**) AlphaFold prediction of the PDAP1 structure showing the canonical 4E-binding motif and serine residues identified as sites of phosphorylation (AlphaFold Protein Structure Database Q13442) (*32*). aa, amino acid. (**B**) Amino acid alignment of PDAP1 with known eIF4E-binding proteins, including 4E-T and C8orf33. The YXXXXLΦ motif is boxed in red, with other conserved Lys/Arg residues boxed in blue. (**C**) Immunoblots of proteins immunoprecipitated (IP) by anti-Flag from lysates of cells expressing PDAP1-Flag or empty vector ("−"), with or without HAV infection. (**D**) Glutathione bead pull-down of bacterially expressed PDAP1 mixed with GST-eIF4E and GST-eIF4E coimmunoprecipitation with PDAP1. Purified recombinant proteins were mixed with a 300-fold molar excess of human serum albumin. (**E**) Immunoblots of proteins pulled down with glutathione beads from lysates of PDAP1-KO1.4 cells expressing PDAP1-Flag, PDAP1-Y124A-Flag, or empty vector ("−") following addition of bacterially expressed GST-eIF4E. sgCtrl, control cells. (**F**) (Left) GFP expressed by the HAV circRNA IRES-GFP reporter in PDAP1-KO1.4 and control cells transfected with PDAP1-Flag, PDAP1-Y124A-Flag or empty vectors ("−"). (Right) Estimated IRES activity calculated as (GFP/GAPDH)/circRNA quantified by RT-PCR. *P* value by two-way ANOVA, $N = 3$ independent experiments. AU, arbitrary units. (**G**) 18f/NLuc reporter virus replication in PDAP1-KO1.4 cells reconstituted with wild-type or Y124A mutant PDAP1. EV, empty vector. (**H**) MS intensities of phosphorylated PDAP1 peptides identified by LC-MS following phospho-peptide enrichment of lysates from mock-infected or HAV-infected Huh-7.5 cells. Data are means of two technical replicates of each of three independent samples. Adjusted *P* value by ANOVA. (**I**) Impact of phospho-mimetic and phospho-ablative mutations on lentivirus-expressed PDAP1-Flag rescue of 18f-NLuc reporter virus replication in PDAP1-KO1.4 cells. *P* values by nonparametric Friedman test with Dunn's correction for multiple comparisons.

translation and replication, might be similarly phospho-regulated. Multiple phosphorylation sites have been identified previously in PDAP1, clustering around residues 17 to 19, 57 to 70, and 172 to 178 (Fig. 3A) (*36*). We found phosphorylation at Ser^{60}, Ser^{63}, and Ser^{176} in a phospho-proteomics analysis of infected and uninfected hepatoma cells, with modest but statistically significant infection-related increases at Ser^{60} and Ser^{63} (Fig. 3H). To assess the significance of phosphorylation, we evaluated the ability of PDAP1-Flag mutants with phospho-mimetic (Asp) or ablative (Ala) substitutions at these residues (and Ser^{19}) to rescue reporter virus replication in PDAP1-KO cells (Fig. 3I and fig. S3B). PDAP1 mutants with Asp substitutions at any of these sites, but particularly Ser^{60}, were more active than unmodified PDAP1 in rescuing replication. S60D also provided greater rescue of HAV circRNA IRES-mediated GFP expression (fig. S3B). Thus, PDAP1 appears to be phospho-regulated in supporting HAV translation and replication.

LFQ proteomics analysis of the PDAP1 interactome

To broadly characterize the PDAP1 interactome, we used label-free quantitative (LFQ) proteomics to identify proteins coimmunoprecipitating with PDAP1-Flag expressed in HAV-infected and uninfected cells (Fig. 4A, top). A total of 646 proteins were identified in in-gel tryptic digests of anti-Flag precipitates, of which 62 were enriched >8-fold in precipitates from cells expressing PDAP1-Flag

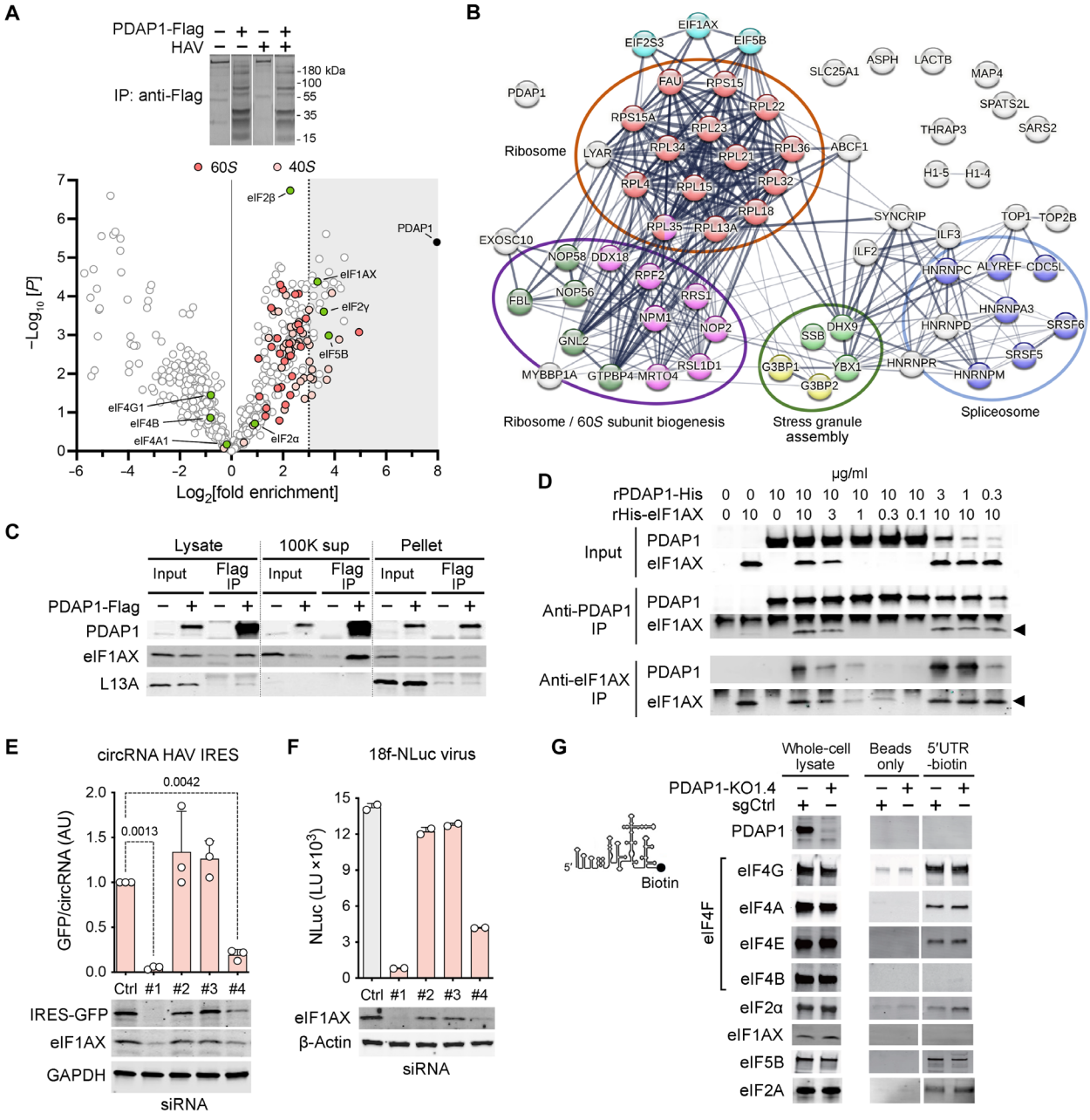

Fig. 4. PDAP1 protein and RNA interactions. (**A**) (Top) SDS-PAGE gel of anti-Flag precipitates from lysates of HAV-infected cells transfected with the empty vector versus PDAP1-Flag expression vector. (Bottom) Volcano plot of proteins identified by LC-MS in in-gel digests of anti-Flag precipitates. (**B**) STRING v12.0 prediction of physical complexes formed by proteins >8-fold enriched in anti-Flag precipitates from cells with or without HAV infection [shaded zone in (A)]. The thickness of connecting lines corresponds to confidence of the physical interaction. Proteins associated with the Kyoto Encyclopedia of Genes and Genomes (KEGG) pathway for ribosome biogenesis are shown in green (hsa03008, $Q = 2.53 \times 10^{-5}$), spliceosome in blue (hsa03040, $Q = 1.69 \times 10^{-6}$) or Gene Ontology (GO) for large ribosome subunit biogenesis in magenta (GO 0042273, $Q = 5.20 \times 10^{-9}$), and stress granule regulation in yellow (GO 0063029, $Q = 7.8 \times 10^{-4}$) or green (GO 1903608, $Q = 5.55 \times 10^{-5}$). (**C**) Immunoblots of anti-Flag precipitates from lysates of cells transfected with the PDAP1-Flag expression vector or empty vector. A postribosome 100K supernatant and ribosome-enriched pellet were generated by high-speed centrifugation. L13A, large ribosomal subunit protein uL13. (**D**) Coimmunoprecipitation of recombinant C-terminally His-tagged rPDAP1-His and N-terminally His-tagged rHis-eIF1A, both produced in bacteria, with anti-PDAP1 or anti-eIF1A. Input mixtures contained a >300-fold molar excess of human serum albumin. (**E**) HAV circRNA IRES reporter activity in cells transfected with four siRNAs targeting *eIF1A* transcripts. Bars show GFP normalized to circRNA abundance. $N = 3$ experiments. *P* values by ANOVA. Below are immunoblots for GFP, eIF1A, and GAPDH (loading control) from a representative experiment. AU, arbitrary units. (**F**) NLuc activity 5 days after quasi-enveloped 18f-NLuc reporter virus infection of cells transfected previously with siRNAs targeting eIF1A. Immunoblots for eIF1A and β-actin (loading control) are shown below. LU, light units. (**G**) Immunoblots of proteins in lysates of sgCtrl and PDAP1-KO1.4 cells coprecipitating with an RNA probe comprising the complete 5′UTR of 18f virus linked to biotin at its 3′ end.

versus control cells transfected with empty vector ($Q < 0.01$) (Fig. 4A, bottom, and table S1). These 62 proteins included the translation initiation factors eIF1A (presumably eIF1AX as Huh-7.5 cells express few eIF1AY transcripts) (*24*), eIF5B, and eIF2γ (eIF2α and eIF2β were enriched four- to sixfold). Other highly enriched proteins included 60*S* and 40*S* ribosome components as well as proteins involved in pre-60*S* subunit biogenesis, stress granule assembly, and mRNA splicing (Fig. 4B). There was little difference in the proteins precipitating with PDAP1 in lysates from infected versus uninfected cells (fig. S3C). In confirmatory experiments, eIF1A, eIF5B, and eIF2α all coimmunoprecipitated with PDAP1-Flag expressed in Huh-7.5 cells (Fig. 3C). Although these are all components of the 43*S* preinitiation complex (PIC), eIF1A coimmunoprecipitated efficiently with PDAP1-Flag from a postribosomal supernatant depleted of ribosomal subunits by high-speed centrifugation (Fig. 4C). Furthermore, recombinant His-tagged eIF1A produced in bacteria coimmunoprecipitated with bacterially expressed His-PDAP1, and vice versa (Fig. 4D), suggesting a direct interaction between these proteins. Unlike eIF4E, the interaction of PDAP1 with eIF1A was not eliminated by the Y124A mutation in the 4E-binding motif (fig. S3D). eIF1A forms specific contacts with eIF5B (suggesting that eIF5B may have been coprecipitated with an eIF1A-PDAP1 complex) (*37*), and in the scanning model of translation initiation, eIF1A and eIF5B function cooperatively to correctly position the 48*S* PIC at the initiator codon prior to 40*S*-60*S* joining (*38*, *39*). Whether eIF1A functions similarly in HAV translation is unknown, but RNA interference (RNAi) knockdown of eIF1A ablated HAV circRNA IRES activity (Fig. 4E) and strongly suppressed replication of the virus (Fig. 4F).

Picornaviral IRES-transactivating factors (ITAFs) like PTBP1 and the La autoantigen are RNA binding proteins that bind to the IRES to up-regulate cap-independent translation (*40*, *41*). By contrast, PDAP1 was not precipitated from hepatoma cell lysates using as bait a 3′ biotinylated 733 nucleotide RNA probe comprising the entire 5′ untranslated region (5′UTR) RNA of HAV (Fig. 4G). Multiple eIF4F subunits (eIF4G, eIF4A, and eIF4E), eIF2α, and eIF5B (but not eIF1A) were all efficiently pulled down with the RNA. Translation factors were equivalently precipitated from lysates of PDAP1-KO1.4 or PDAP1-replete sgCtrl cells (Fig. 4G). Thus, despite previous suggestions that PDAP1 is an RNA binding protein (*42*), it does not associate directly with the HAV IRES in this context.

Stress resistance of PDAP1-dependent HAV translation

As described above, studies in mice suggest a role for PDAP1 in cellular responses to stress (*18*, *19*). Because the overproduction and misfolding of viral proteins may produce ER stress, inducing eIF2α phosphorylation and global repression of protein synthesis (*43*), we asked if HAV translation is stress resistant. To assess this, we transfected a bicistronic HAV IRES reporter into hepatoma cells treated with tunicamycin (Fig. 5, A and B). By inhibiting N-terminal protein glycosylation, tunicamycin induces protein misfolding within the ER, thus activating the protein kinase R (PKR)–like ER kinase (PERK, eukaryotic translation initiation factor 2-alpha kinase 3) that phosphorylates eIF2α (*44*, *45*). As expected, PERK was activated and eIF2α phosphorylated in tunicamycin-treated cells (Fig. 5A), sharply reducing cap-dependent translation of the upstream cistron encoding firefly luciferase (FLuc) in the IRES reporter (Fig. 5B). By contrast, IRES-dependent translation of the downstream cistron encoding *Renilla* luciferase (RLuc) was relatively preserved, resulting in a >50-fold increase in the relative translational efficiency of the IRES (RLuc/FLuc ratio) following eIF2α phosphorylation (Fig. 5B). Similar experiments with the bicistronic IRES reporter revealed that HAV translation was also relatively resistant to sodium arsenite–induced oxidative stress (fig. S4, A and B) as well as infection-related stress in cells infected with chikungunya virus (CHIKV), an RNA virus classified in the Togaviridae family that elicits strong phosphorylation of eIF2α (Fig. 5, C to E).

In the absence of functional GTP-eIF2-Met-tRNA$_i$ ternary complex produced by the phosphorylation of eIF2α, an alternative initiation factor, eIF2A (distinct from eIF2α, the alpha subunit of eIF2), can act cooperatively with eIF5B to deliver tRNA$_i$ for translation initiation (*46*, *47*). Both HAV IRES activity and HAV replication were substantially inhibited by partial eIF2A depletion (fig. S4, C and D), suggesting that eIF2A facilitates Met-tRNAi delivery to HAV RNA. Consistent with this, eIF2A was pulled down from hepatoma cell lysates with the biotinylated HAV IRES bait (Fig. 4G).

Some cellular mRNAs encoding proteins important for cell survival are stress resistant and continue to be translated in the presence of phospho-eIF2α (*35*, *48*). These include proteins such as the heat shock protein family member A5 (ER chaperone BiP), E3 ubiquitin–protein ligase X-linked inhibitor of apoptosis (XIAP), and the proto-oncogene c-Myc, which are encoded by mRNAs containing poorly understood, IRES-like translational elements regulating their synthesis (*48*–*50*). For each of these, we constructed split GFP circRNA reporters similar to the HAV IRES reporter. Translation directed by the XIAP reporter was reduced by 80% ($P < 0.0001$) and BiP translation by 33% ($P < 0.001$) in PDAP1-KO1.4 versus sgCtrl cells, whereas c-Myc translation was not reduced (Fig. 5, F and G). Both BiP and c-Myc translation were highly stress resistant, but c-Myc translation was reduced by 50% in PDAP1-deficient versus PDAP1-replete cells treated with a high concentration of tunicamycin ($P = 0.0069$) (Fig. 5, F and G). Unexpectedly, XIAP translation was strongly reduced by tunicamycin treatment, even in PDAP1-replete cells.

Because stress responses may be aberrant in cancer cell lines such as the Huh-7.5 cells used in these experiments (*51*), we also assessed the impact of PDAP1 deficiency on cellular responses to tunicamycin treatment in $Alb^{Cre+}Pdap1^{f/f}$ mice. Tunicamycin induced PERK activation and eIF2α phosphorylation in the livers of B6 mice, coupled with increased intrahepatic expression of cyclic adenosine 3′,5′-monophosphate–dependent transcription factor 4 (ATF4) and the multifunctional DNA damage-inducible transcript 3 protein [CCAAT/enhancer binding protein homologous protein (CHOP)], as expected (Fig. 6A and fig. S5A) (*43*). By contrast, there was no phosphorylation of eIF2α or increase in ATF4 or CHOP protein abundance in tunicamycin-treated $Alb^{Cre+}Pdap1^{f/f}$ mice. BiP protein, which plays a key regulatory role in the ER stress response (*43*), was also increased by tunicamycin in B6 mice, whereas it was minimally changed in $Alb^{Cre+}Pdap1^{f/f}$ mice (Fig. 6A and fig. S5A). Consistent with the cell culture results (Fig. 5, F and G), XIAP protein expression was strongly reduced in the absence of PDAP1 and not enhanced by stress. Despite the differences in protein abundance, mRNAs encoding BiP, ATF4, and CHOP were comparably increased in tunicamycin-treated $Alb^{Cre+}Pdap1^{f/f}$ and B6 mice (Fig. 6B). Although enhanced protein degradation cannot be excluded, these results suggest impaired translation of BiP, ATF4, and CHOP mRNAs. The lack of a proper adaptive proteostatic response to tunicamycin in the PDAP1-deficient liver was associated histologically with cytoplasmic rarefaction and increased vesiculation of periportal hepatocytes

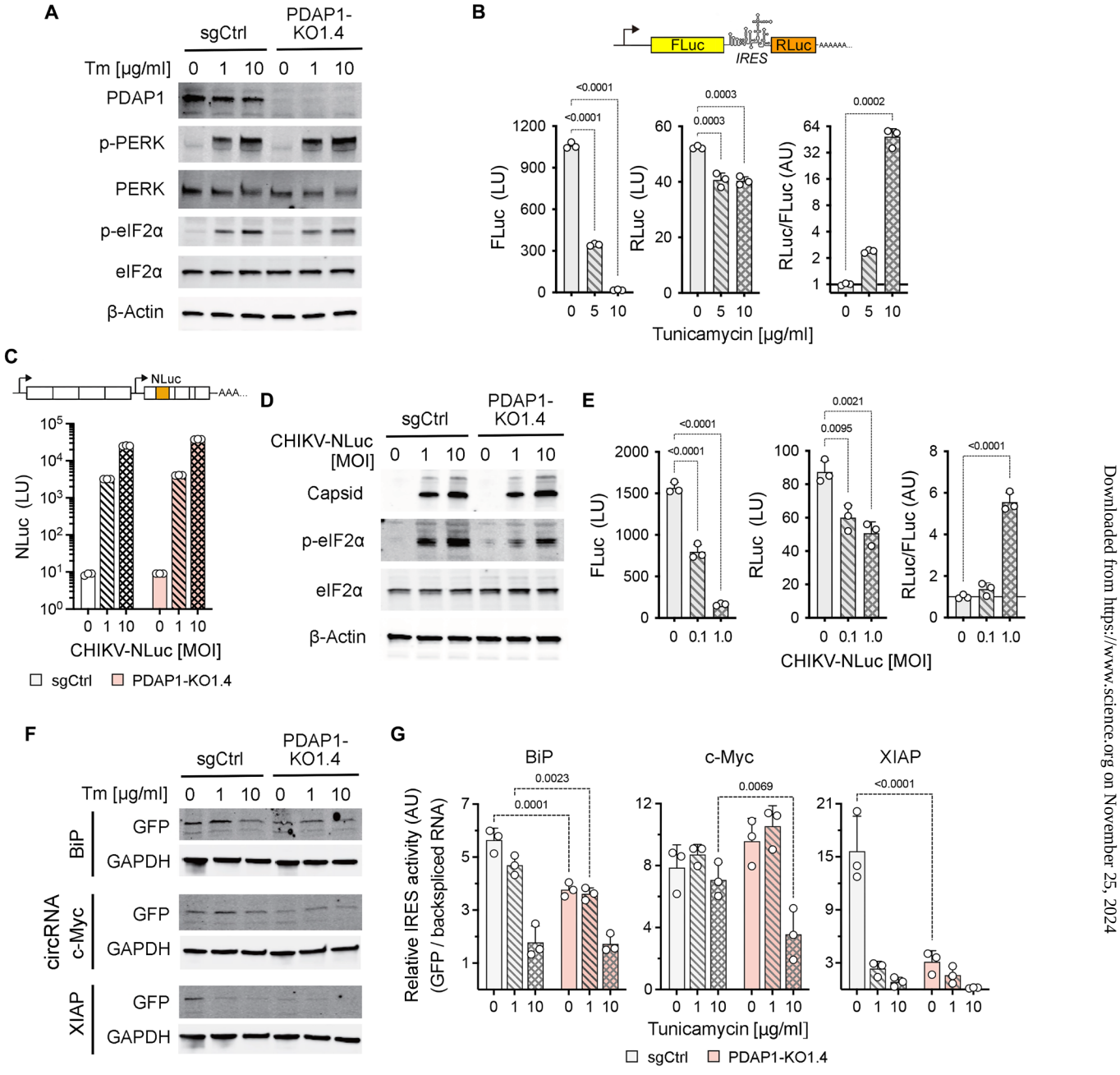

Fig. 5. PDAP1-dependent translation and cell stress. (**A**) Immunoblots of sgCtrl and PDAP1-KO1.4 cell lysates collected 12 hours after tunicamycin (Tm) treatment. (**B**) Dicistronic HAV IRES reporter activity in tunicamycin-treated Huh-7.5 cells. Cells were transfected with plasmid DNA 1 hour after addition of tunicamycin and harvested 24 hours later for FLuc and RLuc assays. $N = 3$ technical replicates from a representative experiment. *P* values by one-way ANOVA. LU, light units; AU, arbitrary units. (**C**) NLuc activity reflecting replication of the CHIKV-NLuc reporter virus in sgCtrl and PDAP1-KO1.4 cells 24 hours after infection. MOI, multiplicity of infection. (**D**) Immunoblots of CHIKV capsid protein, p-eIF2a, and eIF2a in lysates from sgCtrl and PDAP1-KO1.4 cells 24 hours after CHIKV-NLuc infection. (**E**) Dicistronic HAV IRES reporter [see (B)] activity in CHIKV-NLuc–infected sgCtrl cells. Cells were transfected with plasmid DNA 1 hour after infection and harvested 24 hours later for FLuc and RLuc assays. *P* values by one-way ANOVA. Data shown represent $N = 3$ technical replicates. (**F**) Immunoblots of GFP expressed by circRNA IRES reporters containing BiP, c-Myc, and XIAP IRES sequences in tunicamycin-treated sgCtrl versus PDAP1-KO1.4 cells. (**G**) BiP, c-Myc, and XIAP translational efficiencies in sgCtrl and PDAP1-KO1.4 cells, with and without tunicamycin treatment, based on GFP expression normalized to circRNA abundance measured by RT-qPCR. *P* values by two-way ANOVA, with corrections for multiple comparisons using the Benjamini, Krieger, and Yekutieli method. $N = 3$ independent experiments.

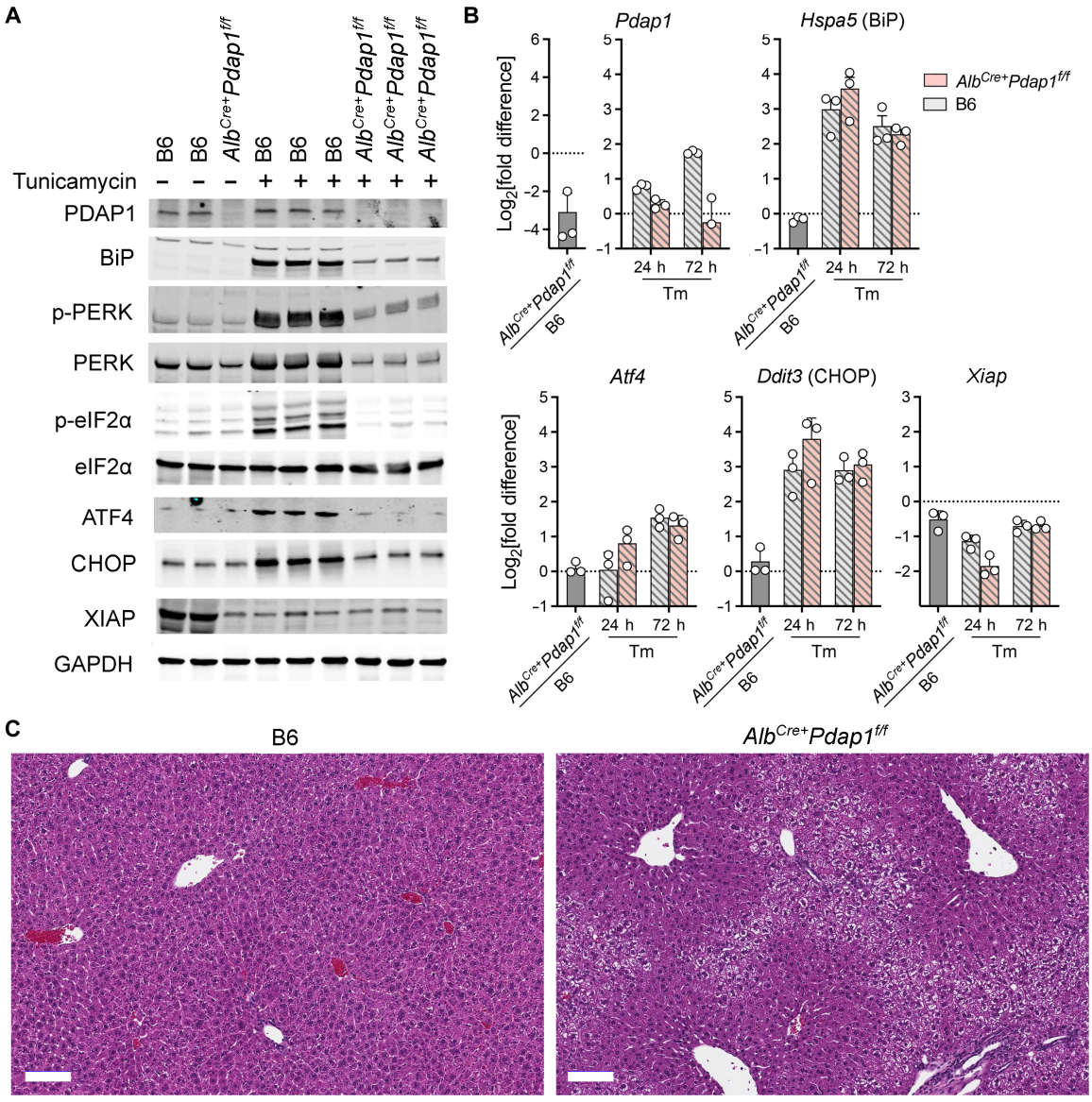

Fig. 6. ER stress response in mice with hepatocyte-targeted *Pdap1* knockout. (**A**) Immunoblots of PDAP1 and stress response–related proteins in liver tissues from *Alb*$^{Cre+}$*Pdap1*$^{f/f}$ and B6 mice 24 hours after intraperitoneal inoculation of a single dose (1 mg/kg) of tunicamycin. (**B**) Fold change in intrahepatic *Pdap1* and stress-related host gene (*Hsap5*, *Atf4*, *Ddit3*, and *Xiap*) transcript levels in B6 and *Alb*$^{Cre+}$*Pdap1*$^{f/f}$ mice, quantified by RT-PCR relative to *Actb* transcript levels, 24 and 72 hours (h) after administration of tunicamycin. Heavily shaded columns on the left represent relative transcript levels in untreated *Alb*$^{Cre+}$*Pdap1*$^{f/f}$ versus B6 mice. Each symbol represents an individual animal. (**C**) H&E-stained sections of liver from (left) B6 or (right) *Alb*$^{Cre+}$*Pdap1*$^{f/f}$ mice 72 hours after administration of tunicamycin. Scale bars, 100 μm.

(Fig. 6C and fig. S5, B and C). Thus, PDAP1 is required not only for HAV IRES activity but also for cytoprotective responses to ER stress in the liver.

DISCUSSION

Taken collectively, our data show that translation of the uncapped, positive-sense RNA genome of HAV is highly stress resistant, persisting despite eIF2α phosphorylation, and dependent on PDAP1, a small phosphoprotein with previously unrecognized eIF4E-binding activity (Figs. 2, E to G, and 3, D and E). Unlike PTBP1 and La protein, both well-studied ITAFs (*40*, *41*), PDAP1 does not bind directly to the HAV IRES (Fig. 4G). It interacts instead with eIF1A and is associated with translating polysomes (Figs. 2G and 4, D and E). eIF1A is known to stabilize Met-tRNAi binding to PICs associated with the HCV IRES, which, like the HAV IRES, is stress resistant (*52*, *53*). eIF1A also facilitates proper start codon recognition by the HCV IRES, particularly in stressed cells (*52*). These actions of eIF1A may be carried out in collaboration with eIF5B, with which it interacts through its C-terminal domain and acts cooperatively to promote 40*S*-60*S* subunit joining (*37*, *39*, *52*). RNAi depletion experiments show that eIF1A is essential for both translation and replication of HAV RNA (Fig. 4, E and F). Whether its capacity to do so is mediated through its interaction with PDAP1 remains to be shown, but it is intriguing to consider the possibility that PDAP1 acts cooperatively with eIF1A to stabilize IRES interactions with the ribosome and facilitate start codon recognition. By contrast,

the inability of the PDAP1-Y124A mutant to rescue HAV translation in PDAP1-KO1.4 cells (Fig. 3, F and G) indicates that the interaction of PDAP1 with eIF4E is crucial to IRES activity. Compelling data support a need for eIF4E in HAV translation (*5*, *6*), although existing models of eIF4E function as the cap-binding component of the eIF4F complex provide little insight into how it might contribute to this cap-independent process. Cell-free biochemical studies suggest that the binding of eIF4E to eIF4G increases the affinity of the eIF4F complex for the HAV IRES and enhances eIF4A unwindase activity on duplex RNA (*54*). However, neither of these eIF4E actions is inhibited by the m^7G cap analog or a W56L mutation in eIF4E that disrupts its cap-binding activity, although both are strongly inhibitory to HAV translation (*5*, *54*).

Our data also show that PDAP1 is essential for basal expression of XIAP protein as well as enhanced BiP, ATF4, and CHOP protein expression in the ER-stressed liver (Fig. 6A and fig. S5A). The lack of expression of these proteins in the PDAP1-deficient liver likely stems from a failure of translation given unchecked stress-related increases in their cognate mRNAs (Fig. 6B). XIAP and, to a lesser extent, BiP and c-Myc translation are also suppressed in PDAP1-deficient hepatoma cells (Fig. 5, F and G). These findings substantially broaden the significance of this study and suggest that PDAP1 is an auxiliary translation initiation factor that may play an important role in hepatocyte survival under conditions of stress. It makes sense that HAV should adopt a PDAP1-dependent mechanism of translation that is stress resistant as this would provide the virus with a survival advantage within hepatocytes in which eIF2α has been phosphorylated by PERK activated by viral proteins in the ER or interferon-inducible PKR activated by double-stranded RNA replication intermediates.

In summary, PDAP1 is essential for HAV translation and thus replication of HAV and hepatitis A pathogenesis. PDAP1 is also necessary for the expression of critical pro-survival proteins in stressed cells. eIF4E, with which it binds (Fig. 3), is limited in abundance and a critical regulator of cellular translation. Hyperactivity of eIF4E has been linked to cell proliferation, presumably by enhancing cellular translation, and is found in many cancers (*55*). While more studies are needed, increased PDAP1 expression has been similarly linked to cancer (*15*–*17*), suggesting the possibility of a shared translation-related mechanism underlying cell proliferation.

MATERIALS AND METHODS

Cells

Human hepatoma-derived Huh-7.5 cells were obtained from Apath LLC. PDAP1-KO cells were generated from Huh-7.5 cells using CRISPR-Cas9–mediated gene editing and PDAP1-targeting lentivector constructs expressing the Brunello library guide sgRNAs #30787(AAAAGCGCAAAGGCGTTGAA) and #30790 (GAGGCAGTATACAAGCCCTG), as described previously (*56*). eIF2A-KO cells were similarly generated using a precloned lentivector construct from Applied Biological Materials (#19073111, sgRNA #2 AAGAGTTTCATCTTCTGACC and sgRNA #3 ACCTGGACCC CAACCATACA). Control sgCtrl cells were similarly transduced with nontargeting sgRNA. Following 2 weeks culture in puromycin (6 μg/ml), single-cell clones (PDAP1-KO1.4 and PDAP1-KO2.1) were isolated by limiting dilution and expanded in puromycin. Clonal eIF2A-KO cells were isolated by limiting dilution. All cell lines tested negative for mycoplasma.

Virus

Cell culture–adapted HAV variants HM175/p16 (p16) and HM175/18f (18f) and the 18f-NLuc reporter virus have been described previously (*21*, *57*, *58*). Murine infections were carried out with mouse-passaged wild-type HM175 strain HAV at the seventh mouse passage (mp7) level. The inoculum was prepared from homogenates of the liver from infected *Mavs*$^{-/-}$ mice, as described previously (*23*). The PV reporter, PV1-NLuc, was constructed by placing the NLuc sequence in-frame between 2C and 3A in the polyprotein-coding sequence of type 1 PV (Mahoney strain). Stocks of plaque-purified LCMV clone 13 (*59*) were prepared from infected BHK-21 monolayers, with infectious titers determined by plaque assay in Vero cell monolayers. The CHIKV-NLuc reporter virus was provided by M. T. Heise of the University of North Carolina at Chapel Hill. It is derived from the 181/25 vaccine strain of CHIKV and expresses NLuc from a sequence placed in-frame between the capsid and E3 envelope-coding sequences, flanked on its C terminus with a sequence encoding the 2A protease of foot-and-mouth disease virus.

Plasmids

Infectious molecular HAV clones pHAV/p16.2 (*60*), pHAV/18f.2 (*60*), p18f-NLuc and p18f-NLuc/GAA (*21*), p18f-FLuc and p18f-FLuc/GAA replicon clones (*58*), pRV-B14-NLuc (*61*), pPV-1/FLuc (*62*) replicons, and bicistronic HAV IRES reporter pFL-HAV-RL (*58*) have been described previously. pPDAP1-Flag, encoding C-terminal Myc/Flag-tagged human PDAP1 (NM_014891.7) under the control of the cytomegalovirus promoter, was purchased from Origene (pRC20058). pPDAP1-Y124 was generated from pPDAP1-Flag by PCR mutagenesis. pMCSG9-PDAP1-Avi, a bacterial expression vector encoding maltose-binding protein fused to PDAP1 with an intervening tobacco etch virus cleavage sequence, was constructed by inserting the PDAP1 sequence from pPDAP1-Flag into pMCSG9 (*63*); a C-terminal GLNDIFEAQKIEWHE Avi tag was added by PCR-based mutagenesis. circRNA reporter plasmids for the EMCV (TR-circGFP), KSHV vFLIP, and PV IRES have been described previously (*64*, *65*). circRNA reporter plasmids containing IRES elements existing in transcripts encoding BiP (HSPA5, GRP78) (NM_005347.5, nucleotides 1 to 220) (*66*), XIAP (NG_007264.1, nucleotides 30293 to 30468) (*67*), and c-Myc (NM_001354870.1, nucleotides 798 to 1205) (*49*) IRES elements were constructed by Gibson assembly using chemically synthesized DNA gene fragments (Genewiz, Azenta). Plasmid constructs were confirmed by whole-plasmid DNA sequencing (Genewiz, Azenta).

Antibodies

The following antibodies were used in these studies: anti-human PDAP1, Proteintech #15081-1-AP; anti-mouse PDAP1, Cell Signaling Technology (CST) #4300; anti-Flag, CST #14793; anti-GFP, Santa Cruz sc-9996; anti-eIF4G, CST #2498; anti-eIF4A, CST #2013; anti-eIF4B, CST #3592; anti-eIF4E, CST #9742; anti-eIF1AX, Proteintech #11649-2-AP; anti-eIF5B, Proteintech #13527-1-AP; anti-4EBP1, CST #9644; anti-eIF2α, CST #5324; anti–phospho-eIF2α, CST #3398; anti-eIF2A, Proteintech #11233-1-AP; anti-XIAP, Proteintech #10037-1-Ig; anti-PPP1R15B, Proteintech #14634-1-AP, anti–β-actin, CST #4967; anti–glyceraldehyde-3-phosphate dehydrogenase (GAPDH), CST #2118; anti-L13A, CST #2765; anti-BiP, CST #3177; anti-PERK, CST #3192; anti–phospho-PERK, CST #3179; anti-ATF4, CST #11815; anti-CHOP, CST #2895; and anti-ISG15, CST #2743. IRDye 800CW and IRDye 680RD conjugated secondary antibodies were obtained from Li-Cor Biosciences.

Chemicals and reagents

Bacterially expressed recombinant PDAP1-6xHis (#ab99246), 6xHis-eIF1AX (#ab101058), and GST-eIF4E (#ab56276) were purchased from Abcam. Guanidine HCl (#G3272), cycloheximide (CHX; #01810), m^7GTP cap analog (#M6113), and WST-1 cell proliferation reagent (#5015944001) were purchased from Sigma-Aldrich. Tunicamycin was from Tocris Bioscience (#3516). Pierce glutathione magnetic agarose beads were purchased from Thermo Fisher Scientific (#78602).

Mice

C57BL/6J (B6) mice were purchased from the Jackson Laboratory (Bar Harbor, Maine). *Ifnar1*$^{-/-}$ mice were bred onto the B6 background and housed under specific pathogen–free conditions, as described previously (*23*). C57BL/6N mice with LoxP sites flanking exon 2 of *Pdap1* (*Pdap1*$^{f/f}$ mice) (*19*) were a gift from M. Di Virgilio of the Max Delbrück Center for Molecular Medicine in Berlin, Germany. These mice were crossed with *Ifnar1*$^{-/-}$ mice to produce doubly homozygous *Pdap1*$^{f/f}$*Ifnar1*$^{-/-}$ mice. *Pdap1*$^{f/f}$ mice and *Pdap1*$^{f/f}$*Ifnar1*$^{-/-}$ mice were bred with B6.Cg-Speer6-ps1$^{Tg(Alb\text{-}cre)21Mgn/J}$ mice ("Alb-Cre" mice, the Jackson Laboratory) to generate *Alb*$^{Cre+}$*Pdap1*$^{f/f}$ and *Alb*$^{Cre+}$*Pdap1*$^{f/f}$*Ifnar1*$^{-/-}$ mice, respectively. *Pdap1* deletion was confirmed in doubly homozygous *Alb*$^{Cre+}$*Pdap1*$^{f/f}$*Ifnar1*$^{-/-}$ mice by immunoblotting of liver tissue. Mice were kept in ventilated cages with standard food and water ad libitum and cared for in accordance with the policies and guidelines of the Institutional Animal Care and Use Committee (IACUC) of the University of North Carolina. All experiments followed the IACUC-approved protocol #21-222.0-A.

Virus infections and tunicamycin treatment of mice

Mice were inoculated with 2×10^6 GE (genome equivalents) or 2×10^7 GE (high-titer inoculum) mp7 HM175 strain HAV, or 2×10^6 plaque-forming units of LCMV clone 13, by tail vein injection at 8 to10 weeks of age (*23*). Mice were housed in individual cages for the collection of fecal pellets and serum samples. Tunicamycin (1 mg/kg body weight) or vehicle control [2% dimethyl sulfoxide in phosphate-buffered saline (PBS)] was administered to mice by intraperitoneal injection. Liver tissue was harvested at necropsy and stored in RNAlater (Thermo Fisher Scientific, #7020), snap frozen on dry ice, and kept at −80°C or fixed in 10% formalin for 48 hours and stored in 70% ethanol for histology. Sections (4 or 5 μm in thickness) cut from the formalin-fixed, paraffin-embedded liver were stained with hematoxylin and eosin (H&E) and examined for histological changes using a bright-field scan scope (Aperio AT2, Leica Biosystems) by a veterinary hepatic pathologist (J.M.C.) who was blinded to experimental conditions.

ALT assay

Mouse sera (2.5 μl) were diluted 1:2 in PBS and assayed for ALT activity by the Reitman-Frankel method using the Alanine Aminotransferase Activity Assay kit (Elabscience, #E-BC-K235-M).

Transfections

Viral and replicon RNAs were transcribed in vitro from plasmid DNA as described previously (*68*). RNA was transfected with the Trans-IT mRNA reagent (Mirus Bio, #MIR 2225) or by electroporation where indicated. Plasmid transfections were carried out using the Lipofectamine 3000 Transfection Reagent (Invitrogen, #L3000008) following the manufacturer's suggested protocol.

RNAi knockdown

Small interfering RNA (siRNAs; four each) targeting eIF1AX (#LQ-011262-01) and a nontargeting control (siCtrl) siRNA pool (#D-001810-10) were purchased from Horizon Discovery. siRNAs were transfected into cells with the Lipofectamine RNAiMax reagent (Thermo Fisher Scientific, #13778075) at a 20 nM final concentration.

RT-qPCR

Total RNA was extracted from cultured cells with the RNeasy Kit (Qiagen) and from mouse liver tissue using TRIzol reagent (Invitrogen Life Technologies). Fecal RNA was isolated using the QIAamp viral RNA isolation kit (Qiagen). HAV and β-actin cDNA synthesis and real-time quantitative PCR (qPCR) were carried out as described previously (*8*, *9*). circRNA reporter transcript cDNA was quantified by qPCR using primers spanning the GFP split in the reporter plasmid: 5′-GCAGTGCTTCAGCCGCTAC-3′ and 5′-GTGTCGCCCTC-GAACTTCAC-3′ (*69*). Cytokine transcripts in liver tissue were quantified as described previously (*69*).

Luciferase reporter assay

Cells were lysed in a 1× passive lysis buffer (Promega, #E1941) for 15 min at room temperature, and lysates were transferred to opaque white 96-well plates (Corning, #3912). NLuc assays were carried out with the NLuc GLOW Assay kit (Nanolight Technology, #325), and FLuc and dual luciferase assays were carried out with the Dual Luciferase Assay Kit (Promega, #E1910). Luminescence was measured using a BioTek Synergy II multimode plate reader (BioTek Instruments).

Immunoblots

Cells were lysed in a radioimmunoprecipitation assay buffer (Millipore, #20-188) for 20 min on ice and then centrifuged at 14,000*g* for 10 min at 4°C. The supernatant fluid was mixed with 4× Laemmli buffer, incubated at 95°C for 5 min, and then resolved in 4 to 15% or 4 to 20% gradient SDS–polyacrylamide gel electrophoresis (PAGE) precast gels (Bio-Rad, #4561086 and #4560196). Proteins were transferred to polyvinylidene fluoride membranes by semidry transfer using the Transblot Turbo apparatus (Bio-Rad). Membranes were blocked in an Odyssey Blocking Buffer (LI-COR Biosciences) and probed with a 1:1000 dilution of primary antibodies overnight, followed by washing in 0.05% Tween 20. Proteins were visualized using an Odyssey Infrared Imaging System (LI-COR Biosciences) after incubation with a 1:10,000 dilution of donkey anti-goat secondary antibodies conjugated with IRDye 800 or IRDye 680 (LI-COR Biosciences) for 1 hour at room temperature, followed by washing with 0.05% Tween 20.

Polysome analysis

sgCtrl control and PDAP1-KO4 cells (2×10^7) were infected with 18f virus [multiplicity of infection = 10] for 5 hours and then harvested for polysome analysis as described previously (*70*). In brief, cells were incubated in media containing cyclohexamide (CHX) (100 μg/ml) for 10 min, washed with PBS containing CHX (100 μg/ml), and harvested by scraping. Cells were pelleted by centrifugation and resuspended in 1 ml of a polysome lysis buffer [140 mM KCl, 5 mM $MgCl_2$, 20 mM tris-HCl (pH 7.4), 0.01% Triton X-100, 10 mM dithiothreitol (DTT), and CHX (100 μg/ml)], placed on ice for 10 min, and then disrupted by multiple passages through a 27-gauge needle. After low-speed centrifugation to remove nuclei, the lysate was

centrifuged at 16,000*g* to remove mitochondria. The clarified cytoplasmic extract was then loaded onto a linear 10 to 50% sucrose gradient and centrifuged in a Beckman SW40 Ti rotor for 2 hours at 32,000 rpm at 4°C. The gradient was fractionated with continuous monitoring of absorbance at OD_{254} (optical density at 254 nm) and individual fractions assayed for HAV and β-actin mRNA by RT-qPCR as described previously (*70*).

[^{35}S]-Met/Cys metabolic labeling

Twenty-four hours after infection with 18f virus at a multiplicity of 100 GE per cell, PDAP1-KO1.4 and sgCtrl cells were starved for 15 min in methionine/cysteine-free medium and then pulse labeled for 30 min with [^{35}S]-labeled L-methionine and L-cysteine (125 μCi [^{35}S]/ml; EasyTag Express Labeling Mix, Revvity, #NEG772002MC). Newly synthesized proteins were quantified following precipitation with 20% trichloroacetic acid, as described previously (*71*).

Biotinylated RNA pull-down

RNA comprising the HAV 5′UTR was transcribed from a PCR-generated template using the MegaScript T7 Kit (Thermo Fisher Scientific, #AM1334) and then biotinylated using the RNA 3′ Biotinylation Kit (Thermo Fisher Scientific, #20160). Ten picomoles of the biotinylated RNA was heated at 75°C for 5 min, cooled to room temperature, and bound to magnetic streptavidin T1 beads (Thermo Fisher Scientific, #65601) using the manufacturer's suggested protocol. Beads were then incubated overnight at 4°C with cytoplasmic lysates of sgCtrl and PDAP1-KO1.4 cells and washed four times with PBS containing 1% Triton X-100. Bound proteins were eluted with an SDS-PAGE sample buffer.

PDAP1 coimmunoprecipitation

For immunoprecipitation of proteins associating with PDAP1 in vivo, Huh-7.5 cells were infected with 18f virus for 3 days, or mock infected, and then harvested in a lysis buffer [150 mM KCl, 25 mM tris-HCl (pH 7.4), 5 mM EDTA, 1% Triton X-100, 5 mM DTT, cOmplete protease inhibitor cocktail (Roche), and RNaseOUT (100 U/ml; Invitrogen)]. Lysates were centrifuged, and supernatants were incubated with anti-PDAP1 (Proteintech, #15081-AP), anti-Flag (CST, #14793), or isotype control immunoglobulin G (IgG) at 4°C for 2 hours, followed by the addition of magnetic Protein G beads (Thermo Fisher Scientific, #88847). Following a 1-hour incubation at 4°C, beads were washed four times in lysis buffer, and proteins were eluted in sample buffer for SDS-PAGE. For proteomics analysis, proteins precipitated with anti-Flag or control IgG were eluted in SDS-PAGE sample buffer and run 1 to 2 cm into an SDS-PAGE gel. The gels were cut, destained, reduced, and alkylated, followed by tryptic digestion. The peptides were extracted, desalted on home-made C18 StageTips, and analyzed by mass spectrometry (MS). There were two biological replicates for each condition (infected versus uninfected and anti-Flag versus control IgG).

Phosphorylated peptide enrichment

Proteins were extracted from triplicate samples of HAV-infected or mock-infected cells in 8 M urea with 50 mM tris-HCl (pH 8.0), then reduced with DTT (5 mM final) for 30 min at room temperature, and alkylated with iodoacetamide (15 mM final) for 45 min in the dark at room temperature. Samples were diluted fourfold with 25 mM tris-HCl (pH 8.0) and 1 mM $CaCl_2$ and digested with trypsin at a 1:100 (w/w, trypsin:protein) ratio overnight at room temperature. Peptides were desalted on a C18 cartridge (Waters), and concentration was measured using the Pierce Quantitative Colorimetric Peptide Assay (Thermo Fisher Scientific). One milligram of each peptide sample was subjected to phospho-enrichment using the High-Select Fe-NTA Phosphopeptide Enrichment Kit (Thermo Fisher Scientific) following the manufacturer's recommended protocol. There were three biological samples for each condition.

MS analysis

Clean peptides were dissolved in 0.1% formic acid and analyzed on a Q Exactive HF-X mass spectrometer coupled with an EASY-nLC 1200 System (Thermo Fisher Scientific, San Jose, CA). Peptides were loaded on to a nanoEase MZ HSS T3 Column (100 Å, 1.8 μm, 75 μm, Waters). A 150-mm-long column was used for in-gel digest samples, and a 250-mm column was used for phosphopeptides. Analytical separation of in-gel digests was achieved with a 45-min gradient. A linear gradient of 5 to 30% buffer B over 29 min and 30 to 45% buffer B over 6 min was executed at a flow rate of 300 nl/min, followed by a ramp to 100% B in 1 min and 9-min wash with 100% B, where buffer A was aqueous 0.1% formic acid, and buffer B was 80% acetonitrile and 0.1% formic acid. Phosphopeptides were separated with a 110-min gradient. A linear gradient of 5 to 30% buffer B over 75 min and 30 to 45% buffer B over 15 min was executed at a flow rate of 300 nl/min, followed by a ramp to 100% B in 1 min and 19-min wash with 100% B.

Liquid chromatography (LC)–MS experiments were also carried out in a data-dependent mode with full MS [externally calibrated to a mass accuracy of <5 parts per million and a resolution of 60,000 at mass/charge ratio (m/z) 200], followed by high-energy collision-activated dissociation tandem mass spectrometry (MS/MS) of the top 15 most intense ions with a resolution of 15,000 at m/z 200. High-energy collision-activated dissociation MS/MS was used to dissociate peptides at a normalized collision energy of 27 eV in the presence of nitrogen bath gas atoms. There were two LC-MS technical replicates for each immnoprecipitate and three replicates for each phosphopeptide sample.

Raw MS data processing and analysis

Mass spectra were processed, and peptide identification was carried out using MaxQuant software version 1.6.10.43 (Max Planck Institute, Germany). All protein database searches were performed against the UniProt human protein sequence database (UP000005640). A false discovery rate for both peptide-spectrum match and protein assignment was set at 1%. Search parameters included up to two missed cleavages at Lys/Arg on the sequence; phosphorylation of tyrosine, serine, and threonine; oxidation of methionine; and protein N-terminal acetylation as a dynamic modification. Carbamidomethylation of cysteine residues was considered as a static modification. Peptide identifications were reported by filtering of reverse and contaminant entries and assigning to their leading razor protein. Label-free quantitation was carried out with MaxQuant. Data processing and statistical analysis were done with Perseus version 1.6.0.7. Protein quantitation was carried out on technical replicates, using two-sample t test statistics with a P value of 0.01 considered a statistically significant fold change in protein abundance for the phosphoproteome and 0.05 for PDAP1 interactors.

Statistical tests

Statistical significance was assessed by two-way t test or analysis of variance (ANOVA) as indicated in the figure legends, with $P < 0.05$

considered significant. Calculations were done using Prism 10 for macOS version 10.2.3 (GraphPad).

Supplementary Materials

The PDF file includes:
Figs. S1 to S5
Legend for table S1
Uncut blot for Figs. 3I and S2G

Other Supplementary Material for this manuscript includes the following:
Table S1

REFERENCES AND NOTES

1. S. M. Lemon, in *Fields Virology: RNA Viruses*, P. M. Howley, D. M. Knipe, Eds. (Wolters Kluwer, ed. 7, 2022), pp. 22–58.
2. E. A. Brown, S. P. Day, R. W. Jansen, S. M. Lemon, The 5′ nontranslated region of hepatitis A virus: Secondary structure and elements required for translation in vitro. *J. Virol.* **65**, 5828–5838 (1991).
3. E. A. Brown, A. J. Zajac, S. M. Lemon, In vitro characterization of an internal ribosomal entry site (IRES) present within the 5′ nontranslated region of hepatitis A virus RNA: Comparison with the IRES of encephalomyocarditis virus. *J. Virol.* **68**, 1066–1074 (1994).
4. L. E. Whetter, S. P. Day, O. Elroy-Stein, E. A. Brown, S. M. Lemon, Low efficiency of the 5′ nontranslated region of hepatitis A virus RNA in directing cap-independent translation in permissive monkey kidney cells. *J. Virol.* **68**, 5253–5263 (1994).
5. I. K. Ali, L. McKendrick, S. J. Morley, R. J. Jackson, Activity of the hepatitis A virus IRES requires association between the cap-binding translation initiation factor (eIF4E) and eIF4G. *J. Virol.* **75**, 7854–7863 (2001).
6. A. M. Borman, Y. M. Michel, K. M. Kean, Detailed analysis of the requirements of hepatitis A virus internal ribosome entry segment for the eukaryotic initiation factor complex eIF4F. *J. Virol.* **75**, 7864–7871 (2001).
7. A. W. Funkhouser, D. E. Schultz, S. M. Lemon, R. H. Purcell, S. U. Emerson, Hepatitis A virus translation is rate-limiting for virus replication in MRC-5 cells. *Virology* **254**, 268–278 (1999).
8. A. Das, R. C. Barrientos, T. Shiota, V. Madigan, I. Misumi, K. L. McKnight, L. Sun, Z. Li, R. M. Meganck, Y. Li, E. Kaluzna, A. Asokan, J. K. Whitmire, M. Kapustina, Q. Zhang, S. M. Lemon, Gangliosides are essential endosomal receptors for quasi-enveloped and naked hepatitis A virus. *Nat. Microbiol.* **5**, 1069–1078 (2020).
9. J. Kulsuptrakul, R. Wang, N. L. Meyers, M. Ott, A. S. Puschnik, A genome-wide CRISPR screen identifies UFMylation and TRAMP-like complexes as host factors required for hepatitis A virus infection. *Cell Rep.* **34**, 108859 (2021).
10. R. Gosert, K. H. Chang, R. Rijnbrand, M. Yi, D. V. Sangar, S. M. Lemon, Transient expression of cellular polypyrimidine-tract binding protein stimulates cap-independent translation directed by both picornaviral and flaviviral internal ribosome entry sites in vivo. *Mol. Cell. Biol.* **20**, 1583–1595 (2000).
11. J. Staring, E. von Castelmur, V. A. Blomen, L. G. van den Hengel, M. Brockman, J. Baggen, H. J. Thibaut, J. Nieuwenhuis, H. Janssen, F. J. M. van Kuppeveld, A. Perrakis, J. E. Carette, T. R. Brummelkamp, PLA2G16, a switch between entry and clearance of Picornaviridae. *Nature* **541**, 412–416 (2017).
12. J. Diep, Y. S. Ooi, A. W. Wilkinson, C. E. Peters, E. Foy, J. R. Johnson, J. Zengel, S. Ding, K. F. Weng, O. Laufman, G. Jang, J. Xu, T. Young, E. Verschueren, K. J. Kobluk, J. E. Elias, P. Sarnow, H. B. Greenberg, R. Hüttenhain, C. M. Nagamine, R. Andino, N. J. Krogan, O. Gozani, J. E. Carette, Enterovirus pathogenesis requires the host methyltransferase SETD3. *Nat. Microbiol.* **4**, 2523–2537 (2019).
13. L. Shen, K. P. Huang, H. C. Chen, F. L. Huang, Molecular cloning and characterization of a novel casein kinase II substrate, HASPP28, from rat brain. *Arch. Biochem. Biophys.* **327**, 131–141 (1996).
14. W. H. Fischer, D. Schubert, Characterization of a novel platelet-derived growth factor-associated protein. *J. Neurochem.* **66**, 2213–2216 (1996).
15. A. Marimuthu, Y. Subbannayya, N. A. Sahasrabuddhe, L. Balakrishnan, N. Syed, N. R. Sekhar, T. V. Katte, S. M. Pinto, S. M. Srikanth, P. Kumar, H. Pawar, M. K. Kashyap, J. Maharudraiah, H. Ashktorab, D. T. Smoot, G. Ramaswamy, R. V. Kumar, Y. Cheng, S. J. Meltzer, J. C. Roa, R. Chaerkady, T. S. Prasad, H. C. Harsha, A. Chatterjee, A. Pandey, SILAC-based quantitative proteomic analysis of gastric cancer secretome. *Proteomics Clin. Appl.* **7**, 355–366 (2013).
16. S. Y. Choi, J. H. Jang, K. R. Kim, Analysis of differentially expressed genes in human rectal carcinoma using suppression subtractive hybridization. *Clin. Exp. Med.* **11**, 219–226 (2011).
17. V. K. Sharma, A. Singh, S. K. Srivastava, V. Kumar, N. L. Gardi, A. Nalwa, A. K. Dinda, P. Chattopadhyay, S. Yadav, Increased expression of platelet-derived growth factor associated protein-1 is associated with PDGF-B mediated glioma progression. *Int. J. Biochem. Cell Biol.* **78**, 194–205 (2016).
18. H. Y. Cui, W. Wei, M. R. Qian, R. F. Tian, X. Fu, H. W. Li, G. Nan, T. Yang, P. Lin, X. Chen, Y. M. Zhu, B. Wang, X. X. Sun, J. H. Dou, J. L. Jiang, L. Li, S. J. Wang, Z. N. Chen, PDGFA-associated protein 1 is a novel target of c-Myc and contributes to colorectal cancer initiation and progression. *Cancer Commun.* **42**, 750–767 (2022).
19. V. Delgado-Benito, M. Berruezo-Llacuna, R. Altwasser, W. Winkler, D. Sundaravinayagam, S. Balasubramanian, M. Caganova, R. Graf, A. Rahjouei, M. T. Henke, M. Driesner, L. Keller, A. Prigione, M. Janz, A. Akalin, M. Di Virgilio, PDGFA-associated protein 1 protects mature B lymphocytes from stress-induced cell death and promotes antibody gene diversification. *J. Exp. Med.* **217**, e20200137 (2020).
20. A. Das, E. E. Rivera-Serrano, X. Yin, C. M. Walker, Z. Feng, S. M. Lemon, Cell entry and release of quasi-enveloped human hepatitis viruses. *Nat. Rev. Microbiol.* **21**, 573–589 (2023).
21. D. Yamane, H. Feng, E. E. Rivera-Serrano, S. R. Selitsky, A. Hirai-Yuki, A. Das, K. L. McKnight, I. Misumi, L. Hensley, W. Lovell, O. Gonzalez-Lopez, R. Suzuki, M. Matsuda, H. Nakanishi, T. Ohto-Nakanishi, T. Hishiki, E. Wauthier, T. Oikawa, K. Morita, L. M. Reid, P. Sethupathy, M. Kohara, J. K. Whitmire, S. M. Lemon, Constitutive expression of interferon regulatory factor 1 drives intrinsic hepatocyte resistance to multiple RNA viruses. *Nat. Microbiol.* **4**, 1096–1104 (2019).
22. L. Sun, H. Feng, I. Misumi, T. Shirasaki, L. Hensley, O. González-López, I. Shiota, W. C. Chou, J. P. Ting, J. M. Cullen, D. O. Cowley, J. K. Whitmire, S. M. Lemon, Viral protease cleavage of MAVS in genetically modified mice with hepatitis A virus infection. *J. Hepatol.* **78**, 271–280 (2023).
23. A. Hirai-Yuki, L. Hensley, D. R. McGivern, O. Gonzalez-Lopez, A. Das, H. Feng, L. Sun, J. E. Wilson, F. Hu, Z. Feng, W. Lovell, I. Misumi, J. P. Ting, S. Montgomery, J. Cullen, J. K. Whitmire, S. M. Lemon, MAVS-dependent host species range and pathogenicity of human hepatitis A virus. *Science* **353**, 1541–1545 (2016).
24. L. Sun, Y. Li, I. Misumi, O. González-López, L. Hensley, J. M. Cullen, D. R. McGivern, M. Matsuda, R. Suzuki, G. C. Sen, A. Hirai-Yuki, J. K. Whitmire, S. M. Lemon, IRF3-mediated pathogenicity in a murine model of human hepatitis A. *PLOS Pathog.* **17**, e1009960 (2021).
25. D. G. Macejak, P. Sarnow, Internal initiation of translation mediated by the 5′ leader of a cellular mRNA. *Nature* **353**, 90–94 (1991).
26. Y. Yang, Z. Wang, Constructing GFP-based reporter to study back splicing and translation of circular RNA. *Methods Mol. Biol.* **1724**, 107–118 (2018).
27. R. M. Meganck, J. Liu, A. E. Hale, K. E. Simon, M. M. Fanous, H. A. Vincent, J. E. Wilusz, N. J. Moorman, W. F. Marzluff, A. Asokan, Engineering highly efficient backsplicing and translation of synthetic circRNAs. *Mol. Ther. Nucleic Acids* **23**, 821–834 (2021).
28. Z. Othman, M. K. Sulaiman, M. M. Willcocks, N. Ulryck, D. J. Blackbourn, B. Sargueil, L. O. Roberts, N. Locker, Functional analysis of Kaposi's sarcoma-associated herpesvirus vFLIP expression reveals a new mode of IRES-mediated translation. *RNA* **20**, 1803–1814 (2014).
29. J. S. Kieft, Viral IRES RNA structures and ribosome interactions. *Trends Biochem. Sci.* **33**, 274–283 (2008).
30. E. González-Almela, H. Williams, M. A. Sanz, L. Carrasco, The initiation factors eIF2, eIF2A, eIF2D, eIF4A, and eIF4G are not involved in translation driven by hepatitis C virus IRES in human cells. *Front. Microbiol.* **9**, 207 (2018).
31. V. Gauss-Muller, F. Deinhardt, Effect of hepatitis A virus infection on cell metabolism in vitro. *Proc. Soc. Exp. Biol. Med.* **175**, 10–15 (1984).
32. J. Jumper, R. Evans, A. Pritzel, T. Green, M. Figurnov, O. Ronneberger, K. Tunyasuvunakool, R. Bates, A. Žídek, A. Potapenko, A. Bridgland, C. Meyer, S. A. A. Kohl, A. J. Ballard, A. Cowie, B. Romera-Paredes, S. Nikolov, R. Jain, J. Adler, T. Back, S. Petersen, D. Reiman, E. Clancy, M. Zielinski, M. Steinegger, M. Pacholska, T. Berghammer, S. Bodenstein, D. Silver, O. Vinyals, A. W. Senior, K. Kavukcuoglu, P. Kohli, D. Hassabis, Highly accurate protein structure prediction with AlphaFold. *Nature* **596**, 583–589 (2021).
33. J. Marcotrigiano, A. C. Gingras, N. Sonenberg, S. K. Burley, Cap-dependent translation initiation in eukaryotes is regulated by a molecular mimic of eIF4G. *Mol. Cell* **3**, 707–716 (1999).
34. A. Bah, R. M. Vernon, Z. Siddiqui, M. Krzeminski, R. Muhandiram, C. Zhao, N. Sonenberg, L. E. Kay, J. D. Forman-Kay, Folding of an intrinsically disordered protein by phosphorylation as a regulatory switch. *Nature* **519**, 106–109 (2015).
35. A. G. Hinnebusch, I. P. Ivanov, N. Sonenberg, Translational control by 5′-untranslated regions of eukaryotic mRNAs. *Science* **352**, 1413–1416 (2016).
36. P. V. Hornbeck, B. Zhang, B. Murray, J. M. Kornhauser, V. Latham, E. Skrzypek, PhosphoSitePlus, 2014: Mutations, PTMs and recalibrations. *Nucleic Acids Res.* **43**, D512–D520 (2015).
37. D. S. Olsen, E. M. Savner, A. Mathew, F. Zhang, T. Krishnamoorthy, L. Phan, A. G. Hinnebusch, Domains of eIF1A that mediate binding to eIF2, eIF3 and eIF5B and promote ternary complex recruitment in vivo. *EMBO J.* **22**, 193–204 (2003).
38. T. V. Pestova, S. I. Borukhov, C. U. Hellen, Eukaryotic ribosomes require initiation factors 1 and 1A to locate initiation codons. *Nature* **394**, 854–859 (1998).

39. C. P. Lapointe, R. Grosely, M. Sokabe, C. Alvarado, J. Wang, E. Montabana, N. Villa, B. S. Shin, T. E. Dever, C. S. Fraser, I. S. Fernández, J. D. Puglisi, eIF5B and eIF1A reorient initiator tRNA to allow ribosomal subunit joining. *Nature* **607**, 185–190 (2022).
40. S. L. Hunt, R. J. Jackson, Polypyrimidine-tract binding protein (PTB) is necessary, but not sufficient, for efficient internal initiation of translation of human rhinovirus-2 RNA. *RNA* **5**, 344–359 (1999).
41. M. Costa-Mattioli, Y. Svitkin, N. Sonenberg, La autoantigen is necessary for optimal function of the poliovirus and hepatitis C virus internal ribosome entry site in vivo and in vitro. *Mol.Cell Biol.* **24**, 6861–6870 (2004).
42. X. X. Zhu, J. H. Li, X. Ni, X. Wu, X. Hou, Y. X. Li, S. J. Li, W. Zhao, X. Y. Yin, Pancreatic ductal adenocarcinoma cells regulated the gemcitabine-resistance function of CAFs by LINC00460. *Cancer Sci.* **113**, 3735–3750 (2022).
43. H. Malhi, R. J. Kaufman, Endoplasmic reticulum stress in liver disease. *J. Hepatol.* **54**, 795–809 (2011).
44. C. Hetz, The unfolded protein response: Controlling cell fate decisions under ER stress and beyond. *Nat. Rev. Mol. Cell Biol.* **13**, 89–102 (2012).
45. M. Costa-Mattioli, P. Walter, The integrated stress response: From mechanism to disease. *Science* **368**, eaat5314 (2020).
46. A. A. Komar, W. C. Merrick, A retrospective on eIF2A-and not the alpha subunit of eIF2. *Int. J. Mol. Sci.* **21**, 2054 (2020).
47. E. Kim, J. H. Kim, K. Seo, K. Y. Hong, S. W. A. An, J. Kwon, S. V. Lee, S. K. Jang, eIF2A, an initiator tRNA carrier refractory to eIF2α kinases, functions synergistically with eIF5B. *Cell. Mol. Life Sci.* **75**, 4287–4300 (2018).
48. N. Thakor, M. Holcik, IRES-mediated translation of cellular messenger RNA operates in eIF2α- independent manner during stress. *Nucleic Acids Res.* **40**, 541–552 (2012).
49. C. Nanbru, I. Lafon, S. Audigier, M. C. Gensac, S. Vagner, G. Huez, A. C. Prats, Alternative translation of the proto-oncogene c-myc by an internal ribosome entry site. *J. Biol. Chem.* **272**, 32061–32066 (1997).
50. Q. Yang, P. Sarnow, Location of the internal ribosome entry site in the 5′ non-coding region of the immunoglobulin heavy-chain binding protein (BiP) mRNA: Evidence for specific RNA-protein interactions. *Nucleic Acids Res.* **25**, 2800–2807 (1997).
51. M. Pizzinga, R. F. Harvey, G. D. Garland, R. Mordue, V. Dezi, M. Ramakrishna, A. Sfakianos, M. Monti, T. E. Mulroney, T. Poyry, A. E. Willis, The cell stress response: Extreme times call for post-transcriptional measures. *Wiley Interdiscip. Rev. RNA* **11**, e1578 (2020).
52. Z. A. Jaafar, A. Oguro, Y. Nakamura, J. S. Kieft, Translation initiation by the hepatitis C virus IRES requires eIF1A and ribosomal complex remodeling. *Elife* **5**, e21198 (2016).
53. J. H. Kim, S. M. Park, J. H. Park, S. J. Keum, S. K. Jang, eIF2A mediates translation of hepatitis C viral mRNA under stress conditions. *EMBO J.* **30**, 2454–2464 (2011).
54. B. C. Avanzino, G. Fuchs, C. S. Fraser, Cellular cap-binding protein, eIF4E, promotes picornavirus genome restructuring and translation. *Proc. Natl. Acad. Sci. U.S.A.* **114**, 9611–9616 (2017).
55. N. Siddiqui, N. Sonenberg, Signalling to eIF4E in cancer. *Biochem. Soc. Trans.* **43**, 763–772 (2015).
56. A. Das, A. Hirai-Yuki, O. Gonzalez-Lopez, B. Rhein, S. Moller-Tank, R. Brouillette, L. Hensley, I. Misumi, W. Lovell, J. M. Cullen, J. K. Whitmire, W. Maury, S. M. Lemon, TIM1 (HAVCR1) Is not essential for cellular entry of either quasi-enveloped or naked hepatitis A virions. *mBio* **8**, e00969–e00917 (2017).
57. R. W. Jansen, J. E. Newbold, S. M. Lemon, Complete nucleotide sequence of a cell culture-adapted variant of hepatitis A virus: Comparison with wild-type virus with restricted capacity for in vitro replication. *Virology* **163**, 299–307 (1988).
58. M. Yi, S. M. Lemon, Replication of subgenomic hepatitis A virus RNAs expressing firefly luciferase is enhanced by mutations associated with adaptation of virus to growth in cultured cells. *J. Virol.* **76**, 1171–1180 (2002).
59. M. Matloubian, T. Somasundaram, S. R. Kolhekar, R. Selvakumar, R. Ahmed, Genetic basis of viral persistence: Single amino acid change in the viral glycoprotein affects ability of lymphocytic choriomeningitis virus to persist in adult mice. *J. Exp. Med.* **172**, 1043–1048 (1990).
60. O. Gonzalez-Lopez, E. E. Rivera-Serrano, F. Hu, L. Hensley, K. L. McKnight, J. Ren, D. I. Stuart, E. E. Fry, S. M. Lemon, Redundant late domain functions of tandem VP2 YPX_3L motifs in nonlytic cellular egress of quasi-enveloped hepatitis A virus. *J. Virol.* **92**, e01308–e01318 (2018).
61. K. L. McKnight, K. V. Swanson, K. Austgen, C. Richards, J. K. Mitchell, D. R. McGivern, E. Fritch, J. Johnson, K. Remlinger, M. Magid-Slav, M. Kapustina, S. You, S. M. Lemon, Stimulator of interferon genes (STING) is an essential proviral host factor for human rhinovirus species A and C. *Proc. Natl. Acad. Sci. U.S.A.* **117**, 27598–27607 (2020).
62. J. Herold, R. Andino, Poliovirus RNA replication requires genome circularization through a protein-protein bridge. *Mol. Cell* **7**, 581–591 (2001).
63. M. I. Donnelly, M. Zhou, C. S. Millard, S. Clancy, L. Stols, W. H. Eschenfeldt, F. R. Collart, A. Joachimiak, An expression vector tailored for large-scale, high-throughput purification of recombinant proteins. *Protein Expr. Purif.* **47**, 446–454 (2006).
64. H. A. Vincent, B. Ziehr, E. M. Lenarcic, N. J. Moorman, Human cytomegalovirus pTRS1 stimulates cap-independent translation. *Virology* **537**, 246–253 (2019).
65. Y. Wang, Z. Wang, Efficient backsplicing produces translatable circular mRNAs. *RNA* **21**, 172–179 (2015).
66. C. Thoma, G. Bergamini, B. Galy, P. Hundsdoerfer, M. W. Hentze, Enhancement of IRES-mediated translation of the c-myc and BiP mRNAs by the poly(A) tail is independent of intact eIF4G and PABP. *Mol. Cell* **15**, 925–935 (2004).
67. M. Holcik, C. Lefebvre, C. Yeh, T. Chow, R. G. Korneluk, A new internal-ribosome-entry-site motif potentiates XIAP-mediated cytoprotection. *Nat. Cell Biol.* **1**, 190–192 (1999).
68. D. Yamane, D. R. McGivern, E. Wauthier, M. Yi, V. J. Madden, C. Welsch, I. Antes, Y. Wen, P. E. Chugh, C. E. McGee, D. G. Widman, I. Misumi, S. Bandyopadhyay, S. Kim, T. Shimakami, T. Oikawa, J. K. Whitmire, M. T. Heise, D. P. Dittmer, C. C. Kao, S. M. Pitson, A. H. Merrill Jr., L. M. Reid, S. M. Lemon, Regulation of the hepatitis C virus RNA replicase by endogenous lipid peroxidation. *Nat. Med.* **20**, 927–935 (2014).
69. Y. Li, I. Misumi, T. Shiota, L. Sun, E. M. Lenarcic, H. Kim, T. Shirasaki, A. Hertel-Wulff, T. Tibbs, J. E. Mitchell, K. L. McKnight, C. E. Cameron, N. J. Moorman, D. R. McGivern, J. M. Cullen, J. K. Whitmire, S. M. Lemon, The ZCCHC14/TENT4 complex is required for hepatitis A virus RNA synthesis. *Proc. Natl. Acad. Sci. U.S.A.* **119**, e2204511119 (2022).
70. T. Masaki, K. C. Arend, Y. Li, D. Yamane, D. R. McGivern, T. Kato, T. Wakita, N. J. Moorman, S. M. Lemon, miR-122 stimulates hepatitis C virus RNA synthesis by altering the balance of viral RNAs engaged in replication versus translation. *Cell Host Microbe* **17**, 217–228 (2015).
71. B. Ziehr, H. A. Vincent, N. J. Moorman, Human cytomegalovirus pTRS1 and pIRS1 antagonize protein kinase R to facilitate virus replication. *J. Virol.* **90**, 3839–3848 (2016).

Acknowledgments: We thank A. Hertel-Wulff and A. Tripathy for expert technical assistance, M. Di Virgilio of the Max Delbrück Centrum für Molekulare Medizin for the gift of floxed *Pdap1*^{f} mice, and M. T. Heise of the University of North Carolina at Chapel Hill for CHIKV-NLuc virus. We also thank J. Kieft of the New York Structural Biology Center for helpful discussions. **Funding:** This work was supported by grants from the US National Institutes of Health [R01-AI103083 (S.M.L.), R01-AI131685 (S.M.L.), R01-AI150095 (S.M.L.), R01-AI103311 (N.J.M.), R01-AI169462 (C.E.C.), R21-AG071229 (X.C.), R41-DK133051 (X.C.), and R01-GM133107]; the UNC Pathology Services Core Facility and Molecular Interactions Core, supported by a P30 CA016086 Cancer Center Core Support Grant from the National Cancer Institute to the UNC Lineberger Comprehensive Cancer Center; and the Yamada Science Foundation (T.S.). **Author contributions:** Conceptualization: S.M.L. and N.J.M. Methodology: E.L., L.X., W.G.F., M.L.-A., and Y.L. Investigation: T.S., E.L., I.M., B.Y., A.D., H.K., and M.L.-A. Supervision: C.E.C., X.C., J.K.W., J.A.D., N.J.M., and S.M.L. Reagent provision: W.G.F. and C.E.C. Formal analysis: J.M.C., L.X., and S.M.L. Funding acquisition: S.M.L., N.J.M., and C.E.C. Writing—original draft: T.S. and S.M.L. Writing—final draft: all authors. **Competing interests:** The authors declare that they have no competing interests. **Data and materials availability:** MS proteomics data have been submitted to the ProteomeXchange Consortium via the PRIDE partner repository with the dataset identifier PXD052233. All other data needed to evaluate the conclusions in this paper are present in the paper and/or the Supplementary Materials. Floxed *Pdap1*^{f} mice were provided by M. Di Virgilio of the Max Delbrück Center for Molecular Medicine in the Helmholtz Association, Berlin, Germany, and Huh-7.5 cells were provided by Apath LLC, under the terms of a material transfer agreement.

Submitted 23 May 2024
Accepted 17 October 2024
Published 20 November 2024
10.1126/sciadv.adq6342